Electromagnetic actuator-structure interaction

Experimentally investigating the coupled dynamic behaviour

A GDP subproject

S.W.H. Weening

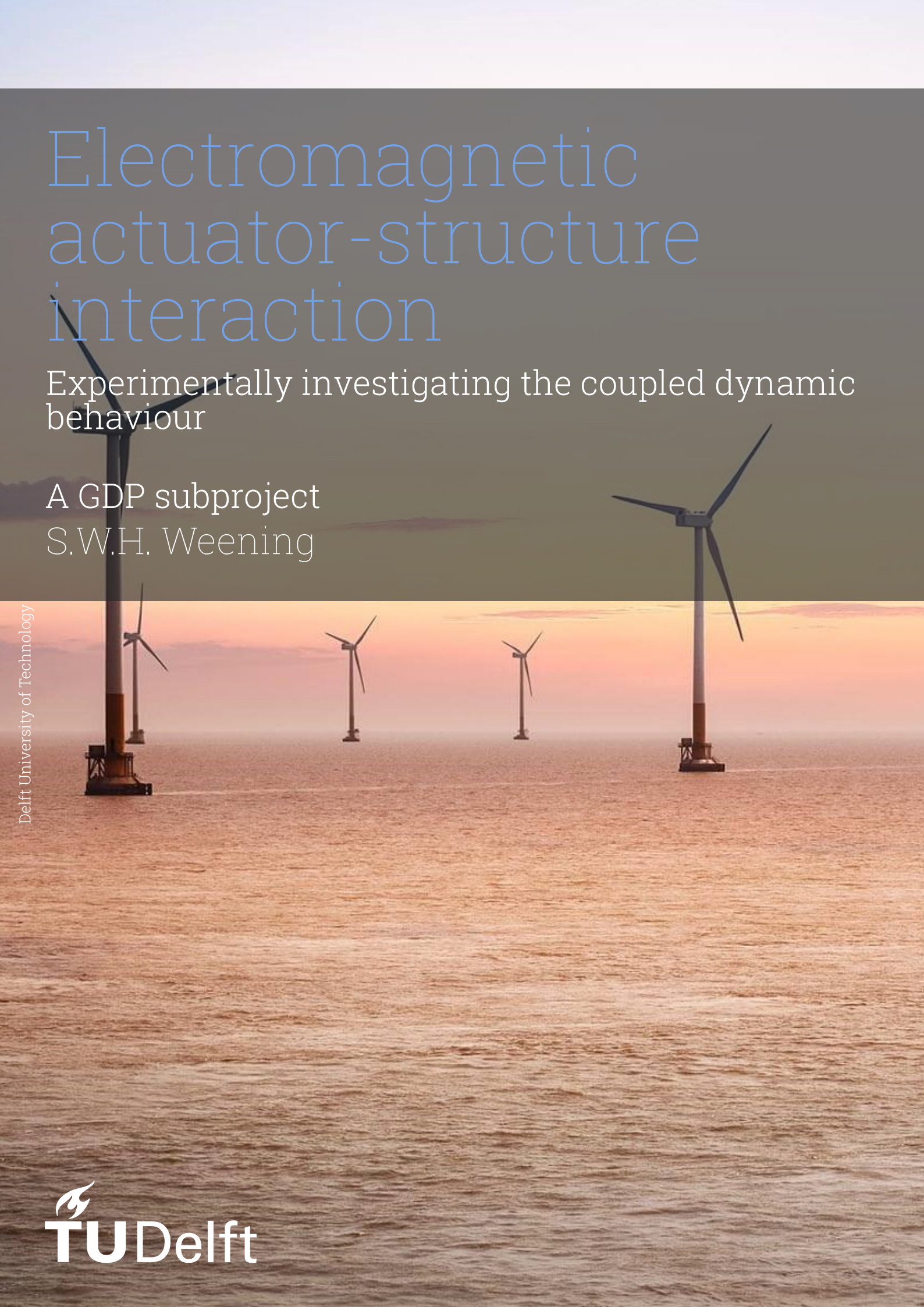

Delft University of Technology

TU Delft

Electromagnetic actuator-structure interaction

Experimentally investigating the coupled dynamic behaviour

by

S.W.H. Weening

Thesis committee:	Prof. dr. A. Metrikine,	Chair assessment committee
	Dr. A. Cabboi,	Assessment committee
	Dr. A. Tsetas,	Daily supervisor
	Dr. S. Gómez	Supervisor
Faculty:	Faculty of CEG, Delft	
Image on cover:	American Clean Power, 2025	

TU Delft

Preface

This thesis was written and submitted to Delft University of Technology in order to achieve the Master of Science degree in Civil Engineering. It is a subproject of the GDP project. From this project came the request to perform research on electromagnetic actuators, in order to determine if they would be suitable to use for the GDP project. The GDP project supplied financing for the purchasing of needed items, e.g. the beam and the actuator.

This report may be of interest for people who want to know more about electromagnetic actuators or about beam dynamics. It will be particularly interesting for people involved in the GDP project. Some pre-knowledge of structural dynamics and data analysis may be useful for understanding the report.

I would like to thank my daily supervisor Dr. Thanasis Tsetas for his good guidance throughout the whole project. I am also grateful to Dr. Sergio Gómez, especially for his help in making the computer model. Prof. dr. Andrei Metrikine helped me a lot with his insights during the progress meetings. I want to thank him for that. This project would not have been possible without the technicians from the Stevinlab and DEMO. I am especially thankful for the help of Jaap Elstgeest, for his large part in building the test setup and for sharing his insights about the project.
In addition to the people directly involved in the project, I would also like to thank a number of people close to me. Firstly, I want to thank my friends from study and from my speed-skating association, DSSV ELS. They provided me with a place to express my enthusiasm, and sometimes frustrations, about the project. Besides that, they were a necessary distraction from the project. I am very grateful to my parents for being such a great support. They always showed interest in my thesis and provided me with useful feedback on my report. And finally, I want to thank my girlfriend, who has always been there to listen to me about anything, from personal matters to the progress of this thesis.

Sybe Weening
Delft, November 2025

Summary

Electromagnetic actuators are an interesting option for inducing vibrations in structures. However, their performance when attached to a flexible structure is relatively unknown. Therefore, this thesis aims to investigate the coupled dynamic behaviour of an electromagnetic actuator and a flexible structure. The goal is to see if the actuator can induce large displacements in the structure, in a controllable manner, and using a small input power.

Physical experiments were performed with an actuator placed on top of a flexible beam. In addition, a computer model was made that could simulate the system and predict its response. In the experiments, multiple input settings for the actuator were tested using frequency sweeps. Two different control settings were compared: the open-loop setting, which controls the current that is sent through the actuator, and the closed-loop setting, which controls the motion of the moving cylinder in the actuator. For both settings, an input signal is sent to the system. Respectively the current or the cylinder motion, relative to the tip of the beam, has to follow that input signal. The amplitude and frequency of the signal can be adjusted.

The experiments showed that there is no perfect input setting. Each setting has its advantages and disadvantages. Therefore, the best input setting to use depends on the situation. Using the open-loop setting at the resonance frequency of the system resulted in large beam tip displacements, a high effectiveness. However, this coincided with a low predictability of the displacements. On the other hand, the closed-loop setting gave a high predictability with a low effectiveness.

Looking at the efficiency of the system, the beam tip displacements normalised by the electrical input power, also did not give an ideal input setting. This was a result of the dynamic behaviour of the beam and the actuator counteracting each other a little. The beam vibrated most efficiently at its resonance frequency. However, this coincided with large relative displacements of the moving cylinder in the actuator. This generated a large Back EMF, causing the actuator to use significantly more electrical power. Thereby, the Back EMF cancels out the efficiency of the resonance. In the closed-loop setting, the relative displacement is being controlled, and therefore it cannot increase to large values. This kills the resonance in the system, preventing the beam tip displacement from increasing.

The computer model was reasonably capable of predicting the response of the system. Due to a few inaccuracies in the model, it often slightly overestimated the displacements of the beam. However, the model showed patterns comparable to the results of the experiments, with resonance peaks at the same frequencies.
The model was also used to simulate the system response to closed-loop settings where either the beam tip displacement or the absolute motion of the cylinder was controlled, instead of the relative motion. These control settings were not possible in the physical experiments, due to limitations in the test setup. However, the model results were promising. Both of these settings could give large beam tip displacements, a high effectiveness, in combination with a high predictability. More research with physical experiments on these settings is recommended.

Contents

1 Introduction

1.1. Research context: The GDP project

Offshore wind turbines are becoming increasingly popular, to accommodate the transition to sustainable energy. Monopiles are often used as foundation for the wind turbines. A monopile is a hollow cylinder made from steel that is driven into the seabed (Wang et al., 2018). With the help of a so-called transition piece, the wind turbine can then be installed on the monopile (Jongen, 2025).

A widely used technique to install the monopile foundations is hammering, pushing the pile down by hitting it on the top. However, this technique has a few disadvantages, such as high forces being exerted on the piles and high levels of underwater noise being produced. The underwater noise and vibrations can cause serious harm to fish and sea mammals (Tougaard and Mikaelsen, 2024). Therefore, governments often impose strict limits on noise production. Not being able to meet these limits could delay or even put a stop to large construction projects (Heerema Marine Contractors, 2024).
Therefore, the GDP (Gentle Driving of Piles) project is aiming to develop a new way of installing monopiles. The piles are driven into the ground by vibrating them both torsionally and vertically. During hammering the thickness of the monopile increases slightly. The impact force from the hammer induces the Poisson effect in the pile, resulting in radial expansion. Torsional vibrations do not induce the Poisson effect. The pile then stays the same diameter and slides into the soil more easily (Metrikine, 2022). The idea is that in this way piles can be installed using less force and causing less nuisance to the surrounding environment. (Nierstrasz, 2023)

1.2. Research problem

For this new technique, vibrations have to be actuated. During the first tests, which are currently already being performed, this is done using hydraulic actuators. Such systems use changes in fluid pressure to generate forces and displacements (Instrumentation Tools, 2024). However, hydraulic actuators have some drawbacks. They require a lot of different parts and create large noises. Therefore, another actuating system is preferred.

Electromagnetic actuators are believed to be the ideal instruments for creating the vibrations. An electric actuator consists of a coil and a permanent magnet. A magnetic field is induced when a current flows through the coil, exerting a force on the magnet (Actuonix Motion Devices, 2024). By placing an alternating current on the coil, a fluctuating motion of the magnet can be created.
Electromagnetic actuators have multiple advantages over hydraulic actuators. They are generally cheaper, more simplistic and create less noise (Duff-Norton, 2022). However, not much is yet known about the controllability of these actuators in this application. Especially when they are put in resonance with a flexible structure, the dynamic behaviour of the combined system is unknown.

1.3. Research aim

This research aims to study the coupled behaviour of an electromagnetic actuator attached to a flexible structure.

1.4. Research scope

This project focuses on the interaction of the electromagnetic actuator with one type of flexible structure, a cantilever beam. The coupled behaviour of the beam-actuator system is analysed by looking at variables related to the vibration of the system, e.g. (natural) frequency and amplitude. The research is aiming to find the influence of this coupled behaviour on the actuator performance. A good performance of the actuator is characterised by the ability to controllably induce large displacements in the beam, while using a low input power.

This research is limited to the use of one type of electromagnetic actuator, MMB 9054 manufactured by Magnetic Innovations (Magnetic Innovations, n.d.).

The main goal of this project is collecting data on the dynamics of the system from physical tests. In addition, the project also focuses on developing a computer model that can predict the deflections of the beam.

1.5. Research questions

Main question

How does the coupled dynamic behaviour between an electromagnetic actuator and a flexible beam influence its performance?

Sub questions

- How can instabilities in the system be prevented?
- To what extent does the Sommerfeld effect play a role in the beam-actuator interaction?
- What elements does a numerical model need to have to be able to accurately predict the response of the beam?
- Which input settings on the actuator result in the best performance?

2

Literature review

This literature review gives an overview of the literature background on some relevant topics for this thesis. The chapter is divided into three main topics: beam theory, the Sommerfeld effect and the electromagnetic actuator. For each topic, the current knowledge is given and its relevance to the thesis is discussed.

2.1. Beam theory

Understanding the behaviour of flexible beams is a widely researched topic. Multiple beam theories have been developed that can describe the deflections of a beam, of which the Timoshenko and the Euler-Bernoulli theories are the most well-known (Öchsner, 2021). This literature study is focused on the Euler-Bernoulli theory, since it is the one that is used in this thesis.

Non-linear vibrations

The Euler-Bernoulli theory uses the assumption of small deflections. The vibrations of the beam-actuator system can be large and thereby might be non-linear, especially when the system is in resonance. Large vibration amplitudes during resonance result in large curvatures in the beam. This leads to a non-linear strain-displacement relationship (Barari et al., 2011).
With this relationship being non-linear, the Euler-Bernoulli equation of motion no longer holds. Therefore, another solution has to be found.

Different solution methods have already been proposed in literature. Tari (Tari, 2013) used Taylor expansion to solve for the deflection, while Du et al. (Du et al., 2018) and Roncen et al. (Roncen et al., 2018) used the harmonic balance method. Das et al. (Das et al., 2012) used the Hamilton principle to obtain the governing equations. Weeger et al. (Weeger et al., 2013) used nonlinear von Kármán strains to calculate the deflections.
Wei et al. (Wei et al., 2020) proposed a solution with large similarity to the topic of this thesis. They used an integration matrix to solve non-linear free vibrations of a horizontally placed cantilever beam with a concentrated mass at the free end.

Roncen et al. (Roncen et al., 2018) performed experiments on the non-linear vibrations of a beam. They found the results to be similar to a Duffing oscillator, with the hardening effect being clearly visible, see figure 2.1.

All of the solutions described above are for slightly different systems than the system this thesis is focused on. Therefore, they would have to be adapted to be able to accurately model large deflections of the beam-actuator system.

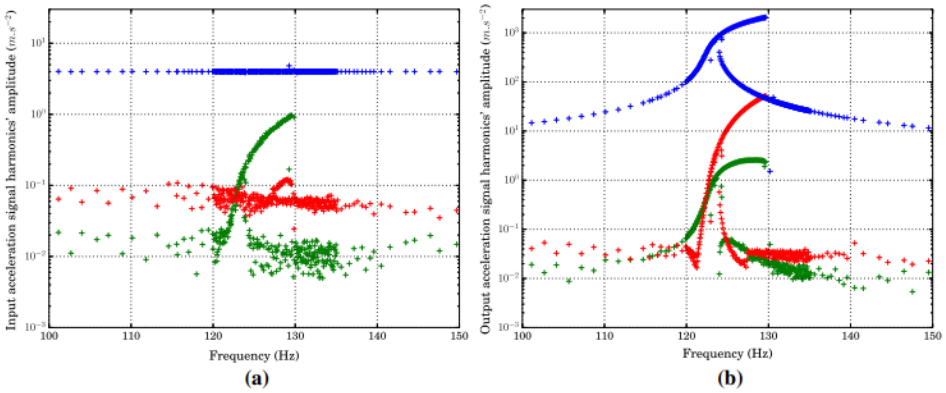

Figure 2.1: Input (a) and output (b) off experimental Harmonics showing the hardening effect (Roncen et al., 2018)

2.2. Sommerfeld effect

The Sommerfeld effect, also known as the resonance capture effect or resonance locking, occurs when a non-ideal energy source is actuating vibrations in a beam. An energy source is called ideal when the source is independent of the rest of the system, i.e. the response of the beam has no influence on the forcing from the energy source (Felix et al., 2009). If this is not the case, the source is non-ideal. In this thesis, the electromagnetic actuator is placed on the free end of a cantilever beam. Therefore, it is likely to be influenced by the vibrations of the beam and be a non-ideal energy source.

When a non-ideal actuator is vibrating close to the eigenfrequency of the system, the system gets trapped in this frequency. The motor is unable to increase the frequency. Instead, the amplitude of the vibration increases. This takes in the extra energy the motor gives while trying to increase the frequency (Gonçalves et al., 2014). Only at a higher frequency, when the motor is inputting enough energy, is it able to escape out of this resonance region. The frequency of the system then jumps to the higher frequency of the motor and the amplitude jumps back to a lower value (Zhang et al., 2021).

Experimental results

Multiple experiments related to the Sommerfeld effect have been performed. Chen et al. (Chen et al., 2024) used frequency sweeps to show the jump phenomena caused by the Sommerfeld effect. They found that the jumps can occur when the frequency is increased as well as when it is decreased. However, the magnitude of the jump can differ depending on the direction of the sweep. Figure 2.2 shows frequency (a) and amplitude (b) jumps that occurred during the frequency sweeps. During the sweeps, the frequency was increased for 250 s, after which it was decreased again. Felix et al. (Felix et al., 2009) showed that the frequency locking and frequency jump can be reduced by increasing the non-linear damping in the system.

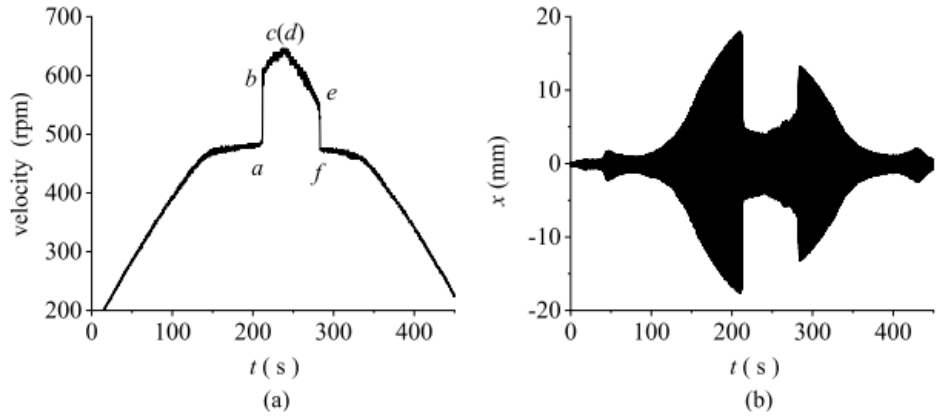

Figure 2.2: Sweep frequency experiment. a Velocity of motor. b Vibration amplitude (Chen et al., 2024)

2.3. Electromagnetic actuator

The actuator that is used in the tests for this project is the MMB 9054 manufactured by Magnetic Innovations. Some research on this actuator has already been done in advance of this project, characterising it and finding its limits (Follet and Weening, 2024).

This research stated that the actuator is reliable at frequencies between 30 and 110 Hz. Furthermore, the temperature should be kept sufficiently low, preferably below 60 $^{\circ}\mathrm{C}$. The temperature can be limited by not letting the actuator run too long at a time, especially at higher currents. In addition, the research showed a clear relationship between the induced Back EMF (electromagnetic force) in the actuator, and the stroke amplitude of the actuator. Back EMF is the effect where the motion of a magnet through the magnetic field of the actuator creates a voltage in the coil. That induced voltage opposes the voltage needed to send the current through the coil. As a result, a higher voltage is required across the actuator. A larger stroke amplitude resulted in a larger amount of Back EMF being generated, causing the voltage across the actuator to increase.

3

Methodology

This chapter discusses the steps that were taken to complete this project. In addition, the test setup is described

3.1. Numerical model

The first step of the project was developing a numerical model that could describe the beam-actuator system. This model was made in Python and was used for multiple purposes. The first use was to help design the beam-actuator system. For the research, it was necessary that the first natural frequency of this system lay within the frequency range of the electromagnetic actuator. The numerical model could predict whether this was the case before the system was actually built.

The second use of the model was to compare the outputs from the model to the results of the lab tests, to check if the model could accurately predict the performance of the system. A more detailed description of the construction and results of the model can be found in chapter 5.

3.2. Test setup

The test setup for the physical experiments was built inside the Stevinlab at TU Delft. A drawing of the design for the setup can be seen in figure 3.1. Figure 3.2 shows a photograph of the eventually built setup. The electromagnetic actuator is connected to the beam through two metal plates which are bolted to both the beam and the actuator. The beam itself is clamped at the bottom in between a thick plate and the Space-frame structure[1].

[1] Space-frames are metal beams with a standard cross-section that can be used to create structures in the Stevin lab. The test setup for this thesis uses a structure made from multiple Space-frame beams.

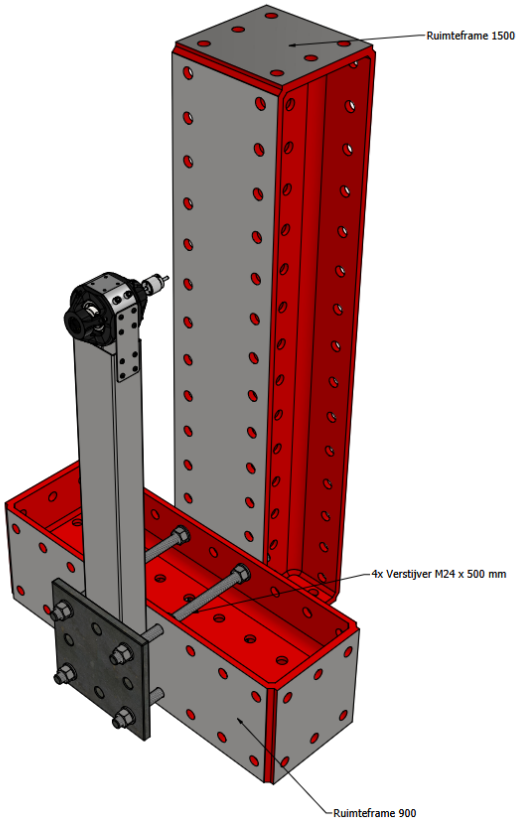

Figure 3.1: Test setup: drawing

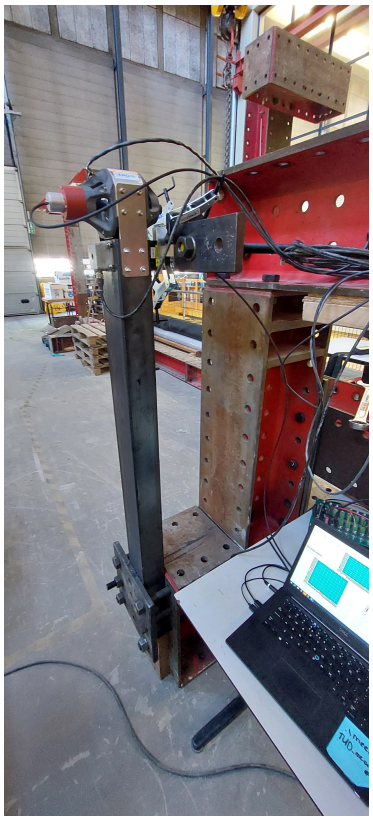

Figure 3.2: Test setup: photograph

3.2.1. Beam

The beam used for the experiments is a steel beam with a hollow rectangular cross-section, 80x120 mm with a thickness of 3 mm. The beam is made of S235 and has a total length of 1.3 m. Of this length, 30 cm is used for the clamping at the bottom, resulting in a free length of 1 m.

The beam is placed with its weak direction aligned with the actuator. This ensures that the beam will mainly vibrate in the direction of interest, since a significantly larger forcing would be needed for vibrations in the strong direction. In this way, instabilities in the other direction are prevented.

3.2.2. Actuator

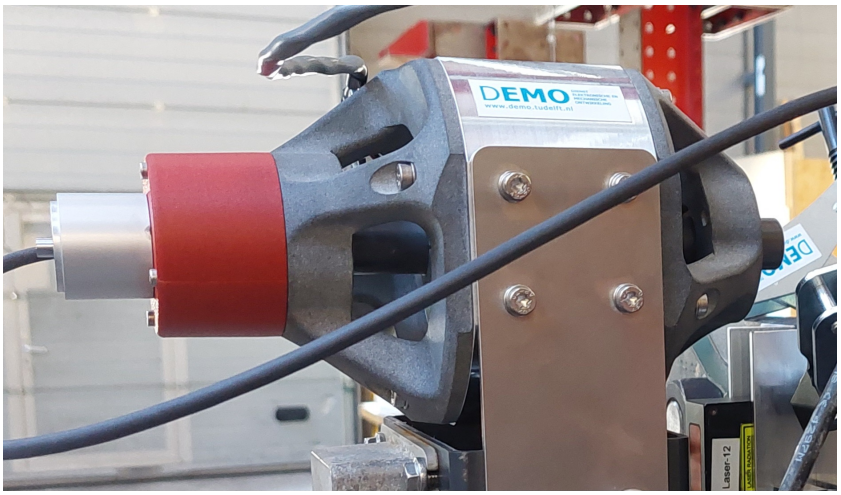

Figure 3.3: Casing actuator

The actuator used in the project is the MMB 9054 linear actuator manufactured by Magnetic Innovations (Magnetic Innovations, n.d.). This actuator consists of a static part containing the coil and a moving cylinder containing the permanent magnet. The actuator is placed inside a custom-made casing, see figure 3.3. The casing houses linear guides for the cylinder and a displacement sensor. The casing is bolted on top of the beam with the use of two connecting plates.

An actuator is often used by attaching the structure that has to be excited to the moving cylinder. If the static part is fixed in place, the force produced by the actuator is directly translated into movement of the cylinder, and thereby movement of the structure. In this project, the beam is not directly connected to the moving cylinder. Instead, it is connected to the casing, and therefore to the static part. The cylinder serves as a counterweight to exert the electromagnetic force on the beam.

3.2.3. Sensors

The test setup includes three different sensors for measuring displacements.

- **Laser sensor**
  The laser sensor is mounted on the Space-frame structure and pointed to the tip of the beam, see figure 3.5. It can measure the displacement of the beam tip.
- **Accelerometer**
  The accelerometer is mounted on the beam, see figure 3.4. It can measure the accelerations of the beam tip.
- **Integrated displacement sensor**
  The casing for the electromagnetic actuator has an integrated displacement sensor, see figure 3.6. This sensor measures the displacement of the moving cylinder in the actuator, relative to the static part of the actuator. This measurement can be combined with the measurement from the laser sensor to determine the absolute displacement of the moving cylinder.

Figure 3.4: Accelerometer

Figure 3.5: Laser sensor

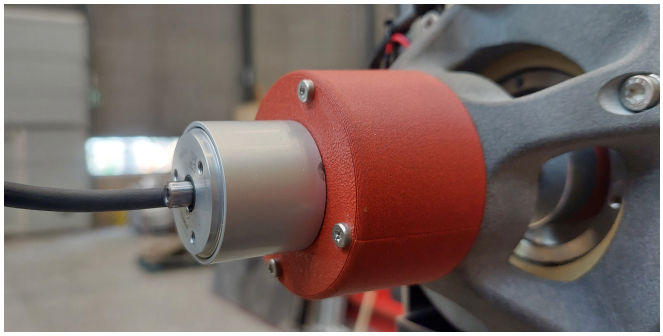

Figure 3.6: Integrated displacement sensor

3.2.4. Controlling the actuator

The electromagnetic actuator is controlled from the MP3 software on a 'meet laptop'[2]. In this software, an input signal can be created which controls the current that is being sent into the actuator. The exact way this controlling works depends on the setting used (open-loop vs closed-loop). The created current signal is sent to a Maxon motor. This motor is the power supply for the actuator and sends the current through the actuator. Figures 3.7 and 3.8 give a schematic overview of the different components involved in controlling the actuator.

Open-loop

In open-loop setting, the input signal is directly translated into the current that is sent to the actuator.

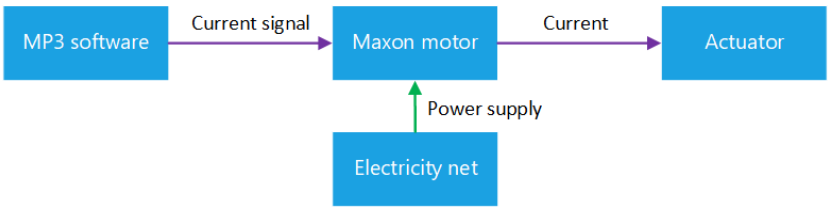

Figure 3.7: Schematic overview open-loop controlling

Closed-loop

The closed-loop setting uses a PID controller to actively control the motion of the moving cylinder relative to the actuator. The input signal in MP3 acts as the target signal, u_{set}, for the PID controller. The controller looks at the difference between this target value and the actual value of the cylinder displacement, measured by the integrated displacement sensor in the actuator. Based on this difference, the

[2]'Meet laptops' or 'meet computers' are computers which can be used for recording measurement data in the Stevin lab. They have access to special software, including MP3.

controller determines the current that has to be sent to the actuator. A more detailed explanation of the working of the PID controller can be found in chapter 5.1.3.

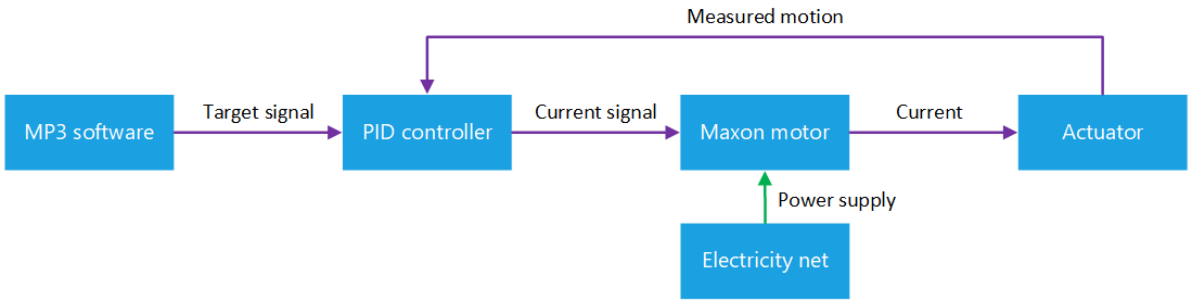

Figure 3.8: Schematic overview closed-loop controlling

3.2.5. Data acquisition

The data from all measurements are gathered in a Data Acquisition Centre (DAQ) and recorded in the MP3 software, using a sampling frequency of 1000 Hz. The data files from the recordings are exported to Python to be processed and analysed.

Table 3.1 gives an overview of the different data channels that are recorded. The test setup did not allow to directly measure the voltage across the actuator. Therefore, the voltages before and after the actuator are measured separately, both relative to the ground. In the processing in Python, Vout2 can be subtracted from Vout1 to calculate the voltage across the actuator.

Table 3.1: Recorded data channels

Channel name	Description	Unit
Displacement rel	The displacement of the moving cylinder relative to the actuator, measured by the integrated displacement sensor	mm
Input current	The current signal that has to be sent to the actuator	A
Output current	The actual current in the actuator	A
Acc_z	The acceleration of the beam tip in the main direction of the movement, measured by the accelerometer	g
Laser	The displacement of the beam tip, measured by the laser sensor	mm
Vout1	The voltage before the actuator, relative to the ground	V
Vout2	The voltage after the actuator, relative to the ground	V

3.3. Experiments

This section talks about the different types of experiments that are used in this project. For each experiment, the method of operation and its function within the project are discussed.

3.3.1. Impact tests

Impact tests are used to determine the natural frequency of the beam-actuator system. The beam is given a pulse excitation by hitting it[3]. After this, the system will mainly vibrate at its natural frequency. These vibrations are recorded and the Time Series are exported to Python. There, a Fourier Transform is applied to the Time Series. This Fourier Transform shows a peak at the natural frequency of the system.

3.3.2. Single frequency tests

Some tests are performed focusing on a single frequency instead of sweeping multiple frequencies. These tests are used to investigate possible instabilities in the beam-actuator system.

3.3.3. Frequency sweeps

The most important experiments in this thesis are frequency sweeps. The sweeps focus on the resonance region of the system, ranging from 40 to 50 Hz with a step size of 0.5 Hz. The frequency sweeps are performed using a Python script that can control the interface of the MP3 software. For each sweep, first the amplitude of the input signal, in amperes for open-loop or in mm for closed-loop, has to be manually set in MP3. Next to that, an empty data file has to be made, in which the recordings can be saved. After that, the script can be run, following the steps below.

For open-loop

- Change frequency to f_i.
  - Start the actuator.
  - Wait for 4 seconds.
  - Record for 8 seconds.
  - Stop the actuator.
  - Wait for 3 seconds.
- Change frequency to f_{i+1}
  - ...

For closed-loop

- Change frequency to f_i.
  - Change PID parameters[a].
  - Start the actuator.
  - Wait for 4 seconds.
  - Record for 8 seconds.
  - Stop the actuator.
  - Wait for 3 seconds.
- Change frequency to f_{i+1}
  - ...

[a] The PID parameters depend on the frequency and amplitude and have to be manually tuned before running the sweep.

The frequency sweeps are performed at multiple amplitudes. For the open-loop setting, the used amplitudes are 2, 3 and 4 amperes. For closed-loop, the amplitudes are 0.5 and 1 mm. For each amplitude, the sweep is repeated five times. When the frequency sweeps are finished, the data files with the recordings can be exported from MP3 to Python to be processed and analysed. The processing for the open-loop tests is carried out separately from the processing of the closed-loop test data. However, the steps taken are the same for both tests.

The data from all the tests are loaded into Python. Each test is loaded as a Pandas DataFrame with each measurement channel as a column and time as index for the rows. After loading, a few extra columns are added to the DataFrame. The channels 'Vout1' and 'Vout2' are used to calculate the voltage over the actuator. This voltage is multiplied by 'Output current' to calculate the electric power used. Next to that, 'Displacement rel' and 'Laser' are added to calculate the absolute displacement of the moving cylinder. The DataFrames for all tests are placed into a single dictionary, categorised by input amplitude.

First, the Time Series of the data channels are plotted to be visually inspected. This is done to check the data for possible mistakes in the measurements. In addition, the plots can be used to spot some trends in the data.

[3] For this thesis the pulse excitation was not applied with an instrumental hammer. Therefore, the input force was not known and it was not possible to make a full FRF of the system. The impact test was solely used to determine the first natural frequency.

After that, the data is processed. The recordings in the DataFrames are for a full frequency sweep consisting of 21 different frequencies. Each DataFrame is split into 21 segments. Every segment is a smaller DataFrame containing all the data from one frequency. The segments are placed in a dictionary. That dictionary is then placed in a larger dictionary 'sweeps_split', containing the data for all the tests.[4] For each segment and each data channel, statistics such as the amplitude are computed. These statistics are plotted against the input frequencies that were used. In this manner, the system can be characterised and the performance of the different input settings can be compared.

The comparison of performance is done based on three main criteria: predictability, effectiveness and efficiency. They are used to compare the different possible input settings.

[4] One segment can be called by typing 'sweeps_split['Testname']['Signal at {Frequency of choice} Hz']'. For example, 'sweeps_split['2A']['Signal at 40.0 Hz'] gives the data for a test at 2 amperes at 40 Hz.

4

Results

This chapter gives the results of the different experiments and analyses that were performed.

4.1. Impact test

Five impact tests were performed. The Fourier Transform from one of them can be seen in figure 4.1. The graph shows a clear peak at the first natural frequency. The location of this peak was checked for all five tests and found to be around 43.5 Hz. The frequencies of the peaks for the individual tests can be found in table 4.1

The graph also has a number of smaller, very sharp, peaks. They are located at the exact multiples of the first natural frequency. These peaks are not likely the next natural frequencies of the system. The natural frequencies of a cantilever beam are not multiples of each other. In addition, a peak from a mode of the system would be wider due to the damping in the system. The smaller peaks could indicate non-linearities in the system, or they could be a side effect of the signal processing.

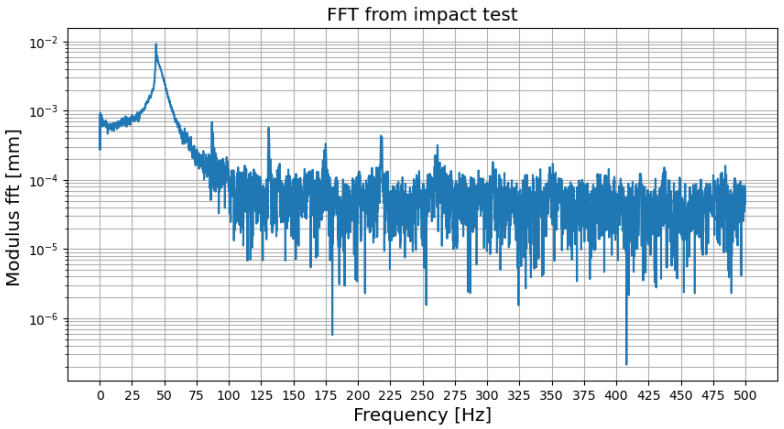

Figure 4.1: FFT from impact test

Table 4.1: Results impact tests

Test	**Natural frequency**
Test 1	43.439 Hz
Test 2	43.529 Hz
Test 3	43.404 Hz
Test 4	43.624 Hz
Test 5	43.645 Hz
Average	**43.528 Hz**

4.2. Frequency sweeps

This section shows the plots that were made from the data of the frequency sweeps and describes the observations that can be made from them. In all plots, the results from individual tests are plotted in thin lines. The bold lines represent the average value per input amplitude. Time series of the frequency sweeps can be found in appendix C.

4.2.1. Beam tip displacement

Open-loop

The plots for the beam tip displacement show a clear difference between the open-loop setting and the closed-loop setting. The open-loop graph shows resonance peaks around 47 Hz. This is a different frequency than the natural frequency found in the impact tests. It turns out that the natural frequency depends on whether the system is operating or not. This has to do with the mass of the moving cylinder working either as a tip mass or as a separate system. During the impact tests, the cylinder acts as an extra tip mass, adding up to the mass of the stator part of the actuator. However, when the actuator is operating during the frequency sweeps, the cylinder moves separately from the beam. This lowers the tip mass on the beam, resulting in a higher natural frequency.

The resonance peaks seem to shift slightly to the left with increasing current. A higher input current, and thus a larger beam displacement, results in a peak at a lower frequency. This could be an indication of non-linearities occurring in the system.

Closed-loop

In the closed-loop graph, an increase in the beam tip displacement can be seen round the frequency of 43.5 Hz. The reason for this is that the closed-loop setting tries to control the relative displacement between the cylinder and the actuator. However, at 43.5 Hz, the natural frequency of the system if the cylinder acts as a tip mass, the cylinder seems to lock in with the rest of the system. Therefore, more force is needed to induce the relative motion. This results in larger beam tip displacements.
Instead of one peak, the graph shows two peaks with a small drop in between. This is due to the parameters of the PID controller. For each frequency in the sweep, these parameters have to be tuned manually. This manual tuning can cause the parameters to not be fully perfect. For 42.5 Hz, the P parameter was slightly too low. This caused the current in the actuator to be lower, see figure 4.9, resulting in a lower beam tip displacement. Having perfectly tuned PID parameters would have likely resulted in a single peak around 43.5 Hz.

The resonance peak around 47 Hz, that can be seen in the graph for open-loop, does not appear in the closed-loop setting. This resonance is accompanied by large relative displacements between the cylinder and the beam tip, large beam tip displacements and small cylinder displacements, see figure 4.10. However, in the closed-loop setting, this relative displacement is being controlled to follow the input signal. Therefore, it cannot increase and the resonance is killed.

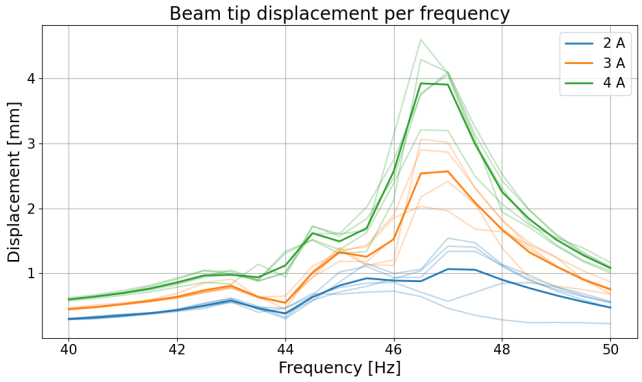

Figure 4.2: Beam tip displacement: open-loop

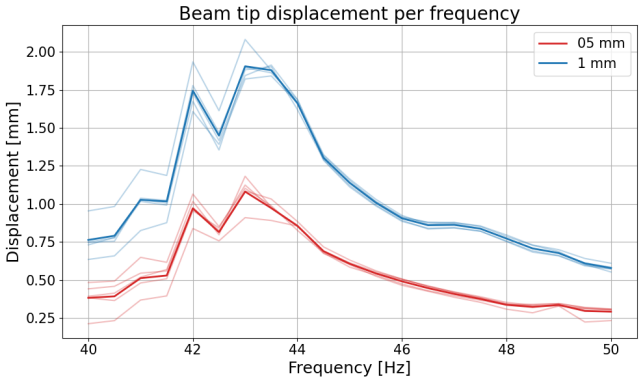

Figure 4.3: Beam tip displacement: closed-loop

4.2.2. Electrical power

Open-loop

The graph for electrical power usage in the open-loop setting has a peak at 47 Hz, the natural frequency of the system in operation. This is due to Back EMF in the actuator. The resonance at 47 Hz coincides with large relative displacements between the cylinder and the coil, see figure 4.10. These large relative displacements mean that a large amount of Back EMF is generated, and the voltage across the actuator increases, see figure 4.6. However, this increase is not enough to fully compensate for the Back EMF. Therefore, the current in the actuator drops below the desired value. The increase in voltage is larger than the decrease in current, resulting in a peak in the electrical power.

Closed-loop

For the closed-loop setting the electrical power usage is significantly large around 43.5 Hz. At this frequency, the locking phenomenon causes a large current to be required in order to generate the desired relative displacement of the cylinder. For this large current, also a large voltage is needed. The combination of a large current and large voltage results in a large electric power.

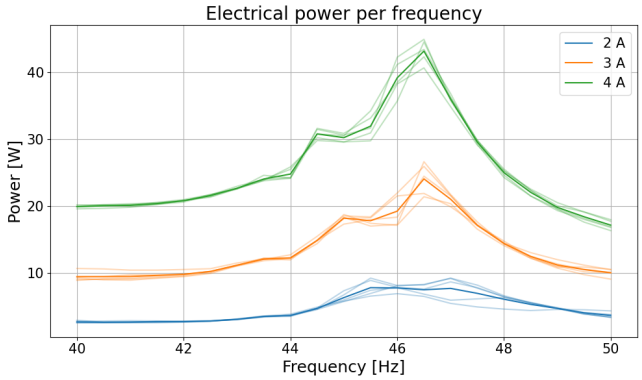

Figure 4.4: Electrical power used: open-loop

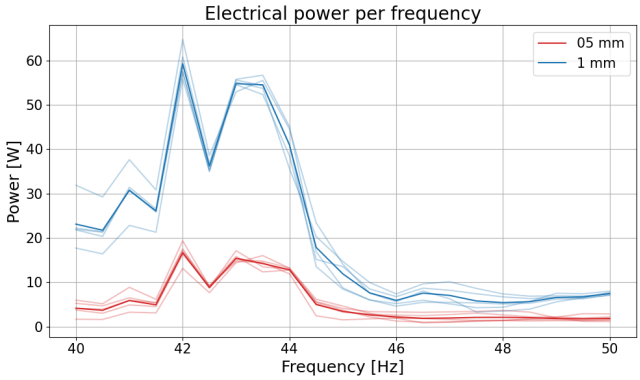

Figure 4.5: Electrical power used: closed-loop

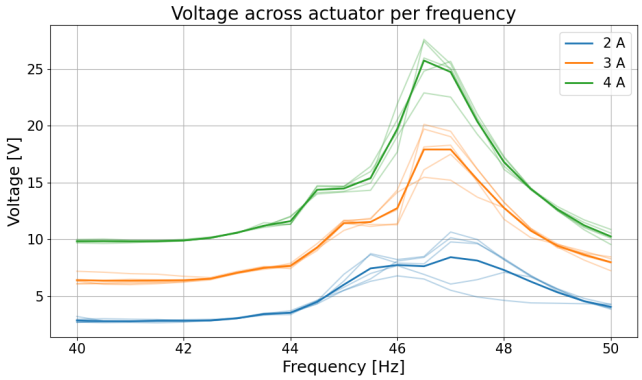

Figure 4.6: Voltage across actuator: open-loop

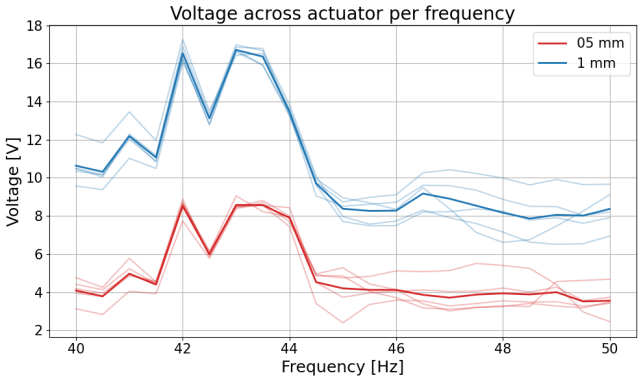

Figure 4.7: Voltage across actuator: closed-loop

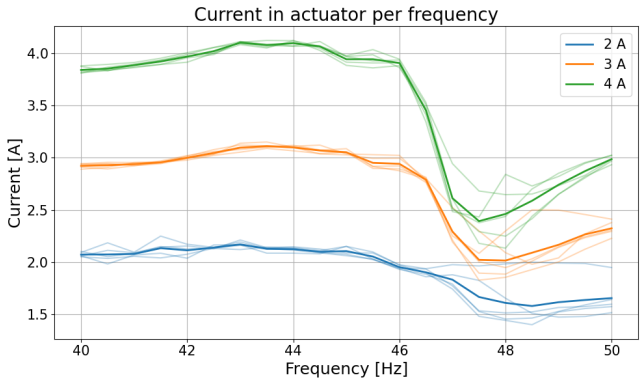

Figure 4.8: Current in actuator: open-loop

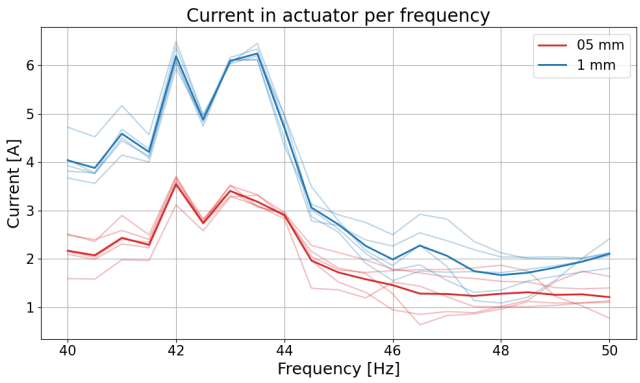

Figure 4.9: Current in actuator: closed-loop

4.2.3. Displacements moving cylinder

Open-loop

The relative displacement between the moving cylinder and the actuator for the open-loop setting shows both natural frequencies of the system. At 43.5 Hz, the relative displacement is very small, due to the locking phenomenon explained in chapter 4.2.1. At 47 Hz the resonance causes the beam tip displacement to increase significantly, see figure 4.2, whereas the absolute displacement of the moving cylinder remains nearly unchanged, see figure 4.12. This results in a large relative displacement.

Closed-loop

In the closed-loop setting, the relative displacement is the variable that is being controlled. However, at frequencies around 43.5 Hz, the actuator was unable to impose the desired displacement. Due to the locking phenomenon, a high current would be required to achieve the desired displacement. This would exceed the limits of the actuator and risk instabilities, see chapter 4.3. At higher frequencies, the controller is better able to produce the desired displacement.

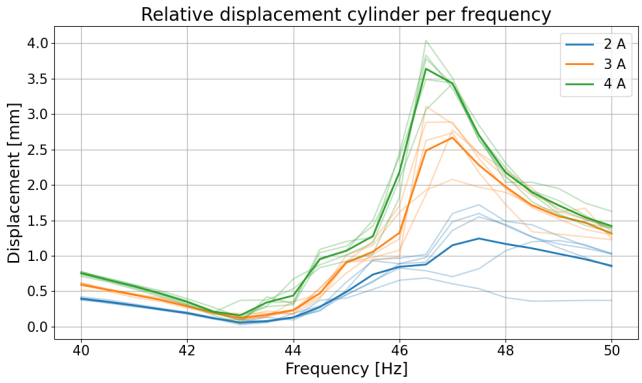

Figure 4.10: Relative displacement moving cylinder: open-loop

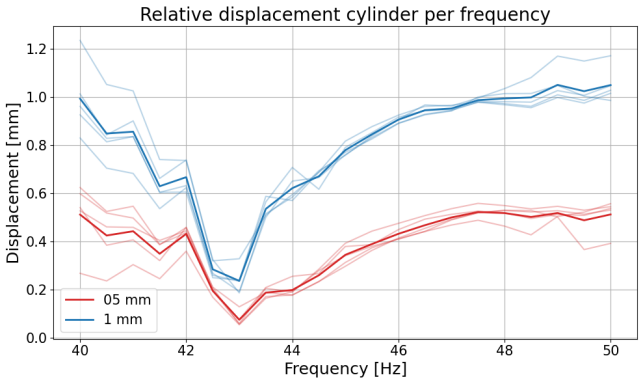

Figure 4.11: Relative displacement moving cylinder: closed-loop

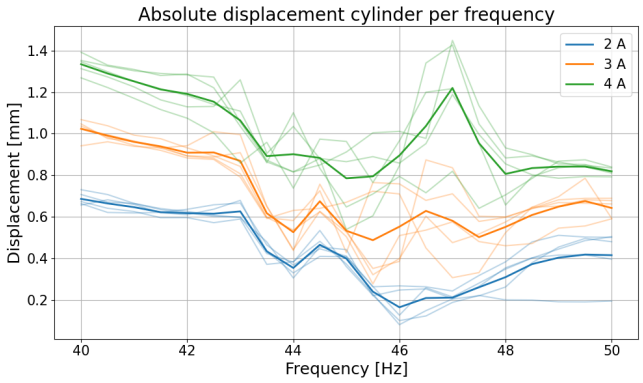

Figure 4.12: Absolute displacement moving cylinder: open-loop

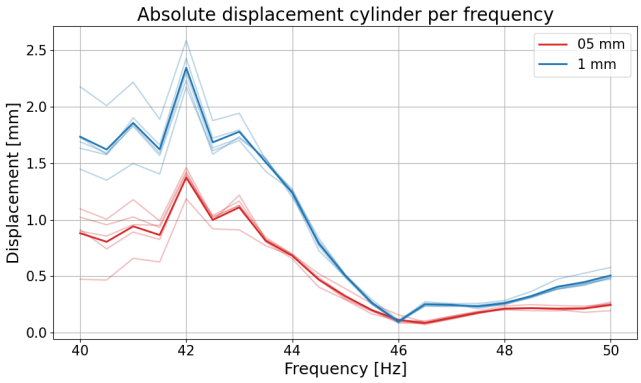

Figure 4.13: Absolute displacement moving cylinder: closed-loop

4.2.4. Efficiency

The efficiency is defined as the beam tip displacement (the output) divided by the electrical power used (the input). For both the open-loop and the closed-loop setting, large beam tip displacement correlates with high electrical power consumption, albeit due to different causes. Therefore, the graphs for efficiency do not show significantly high peaks. However, there is some increase in efficiency visible around the 47 Hz resonance frequency. In addition, using a higher input amplitude appears to result in a lower efficiency.

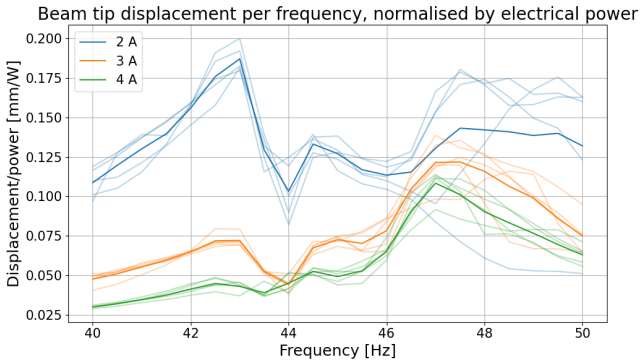

Figure 4.14: Efficiency system: open-loop

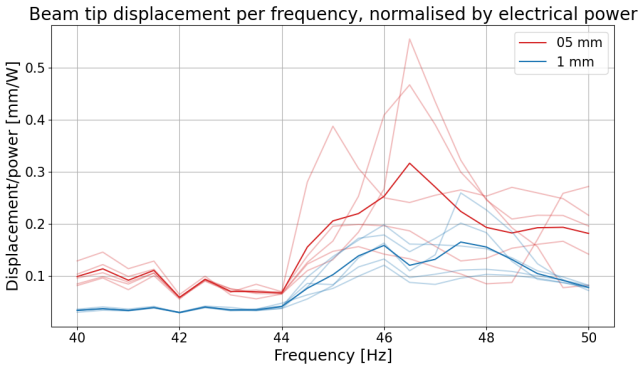

Figure 4.15: Efficiency system: closed-loop

4.2.5. Predictability

For each input amplitude, five tests were performed. Figures 4.16 and 4.17 show the standard deviations of the beam tip displacement in these five tests. This standard deviation can be used as an indication for the predictability of the response of the system. The closed-loop setting has lower standard deviations than the open-loop setting. This difference is particularly visible at the frequencies with large beam tip displacements, 47 Hz for open-loop and 43.5 Hz for closed-loop. The lower standard deviation indicates that the response of the system can be predicted better when using the closed-loop setting.

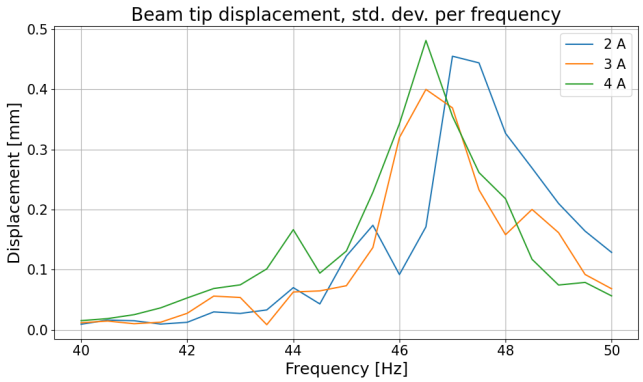

Figure 4.16: Standard deviation beam tip displacement: open-loop

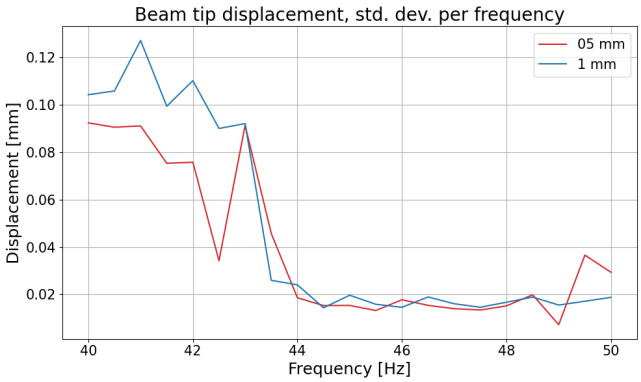

Figure 4.17: Standard deviation beam tip displacement: closed-loop

On the other hand, the standard deviation for the electrical power used is lower for the open-loop setting, see figures 4.18 and 4.19. This indicates that the usage of electrical power is easier to predict when using the open-loop setting. This is self-evident, as this setting controls the current sent to the actuator. The closed-loop setting controls a displacement in the system, making it logical that this setting results in better predictability of the response of the system.

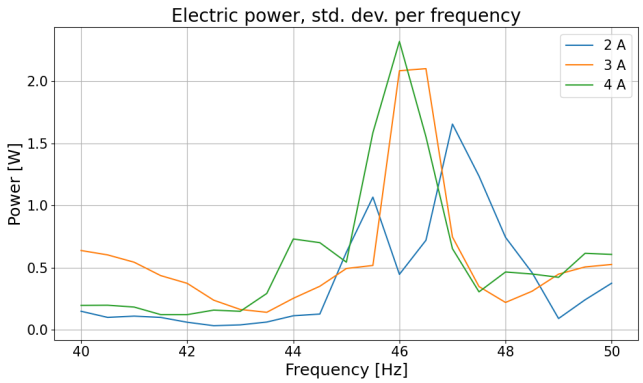

Figure 4.18: Standard deviation electrical power: open-loop

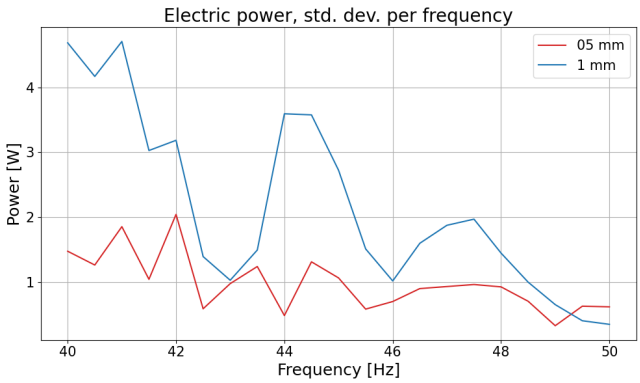

Figure 4.19: Standard deviation electrical power: closed-loop

4.2.6. Phase shift

Figures 4.20 and 4.21 show the phase difference between the movement of the beam tip and the cylinder. Both plots show a shift in the phase difference around 47 Hz, from 0° to approximately 180°. For the open-loop setting, the shift appears to be more gradual than for closed-loop. This indicates that damping is playing a larger role in the open-loop setting. The difference in displacement amplitudes at this frequency could be the cause for this. In open-loop, the resonance at 47 Hz results in large displacements. In closed-loop, the resonance is killed and the displacements remain limited.

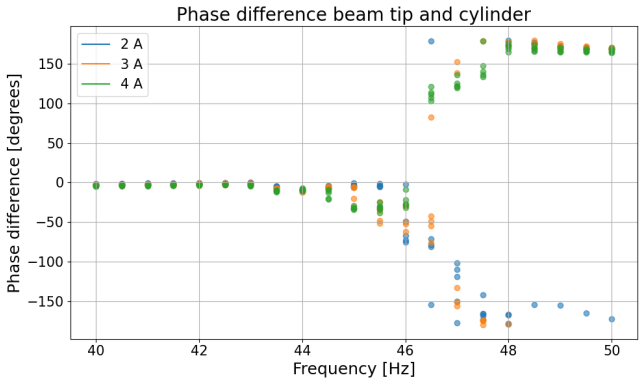

Figure 4.20: Phase difference beam tip-cylinder: open-loop

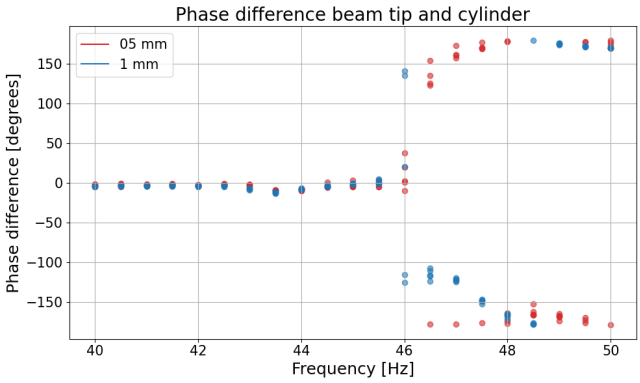

Figure 4.21: Phase difference beam tip-cylinder: closed-loop

4.2.7. Comparing input settings

The input setting used for the actuator can be adjusted in three ways: changing the control setting, changing the frequency, or changing the input amplitude. The control setting can be either open-loop or closed-loop. The frequency has a large range of possible values. The actuator can operate at frequencies between 30 and 110 Hz. However, the frequencies of interest are those around the resonance frequency. For the comparison of the input settings, two frequencies were considered. The resonance frequency found by the impact test, 43.5 Hz, and the resonance frequency when the actuator is in operation, 47 Hz. The input amplitude used depends on the control setting. For open-loop, this is the magnitude of the current signal. A small amplitude, 2 A, or a large amplitude, 4 A, can be used. For the closed-loop setting, the input amplitude is the amplitude of the input signal used for the PID controller. Here, a large amplitude is 1 mm and a small amplitude is 0.5 mm.

Table 4.2 shows the performance of the actuator under the different possible input settings. The performance is assessed based on three criteria: effectiveness[1], predictability[2] and efficiency[3]. Each input setting is given a score between 1 and 5. The scores are placed uniformly over the range of performances. The best performance corresponds with a score of 5, the worst performance with 1. The other scores are placed linearly between them. The settings are rated based on which score their performance is closest to. Each criterion is weighted[4]. Multiplying each score by the weight and adding them up gives the total score in the right column. This score gives an indication of the overall performance of each input setting.

[1] The effectiveness is based on the magnitude of the beam tip displacements. A larger beam tip displacement gives a higher score for effectiveness.

[2] The score for predictability is based on the standard deviations of the beam tip displacement. A lower standard deviation results in a higher score for predictability.

[3] A higher efficiency results in a higher score.

[4] Effectiveness is given a weight of 2, predictability and efficiency have a weight of 1. These weights can be changed depending on the circumstances in which the actuator has to be used.

Table 4.2: Performance input settings actuator (numerical scale)

Input settings			Performance			
Control setting	**Frequency**	**Input amplitude**	**Effectiveness**	**Predictability**	**Efficiency**	**Weighted score**
Open-loop	43.5 Hz	Small current	1	4	4	**10**
		Large current	2	3	1	**8**
	47.0 Hz	Small current	2	1	4	**9**
		Large current	5	1	3	**14**
Closed-loop	43.5 Hz	Small amplitude	2	3	2	**9**
		Large amplitude	3	3	1	**10**
	47.0 Hz	Small amplitude	1	5	5	**12**
		Large amplitude	2	5	4	**13**

4.3. Instabilities

Instabilities can occur in the system when using the closed-loop setting, if the parameters for the PID controller are not tuned correctly. Figures 4.22 and 4.23 show Time Series of a single-frequency test performed using the closed-loop setting. In this test, the value for the P parameter of the PID controller was too high.

Initially, the test ran smoothly. The PID controller was able to create a harmonic relative displacement for the cylinder, following the input signal. However, eventually the amplitude of the vibrations rapidly increased. This had to do with the working of the PID controller. The controller constantly calculates the error, the difference between the actual relative displacement and the desired value. Based on that error, the controller determines the current that needs to be sent to the actuator. This is done according to the control function in equation 5.23, using the parameters as scaling factors. If the value of the P parameter is too high, a slight disturbance, and therefore a slight increase in the error, can cause the controller to overshoot. It tries to correct the error by adjusting the current that is sent to the actuator. With a too high P parameter, this current will also be too high. This results in an even larger error, creating a vicious circle in which the amplitudes of the current and the displacements rapidly increase.

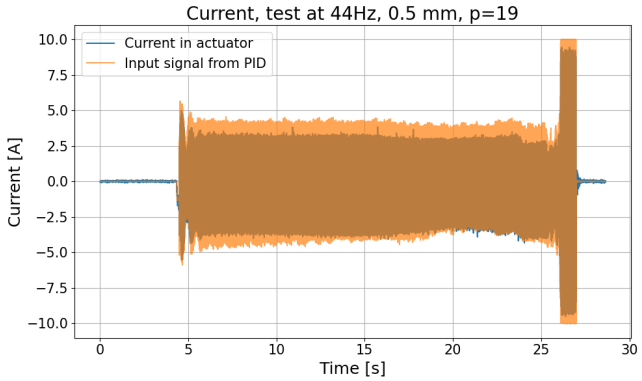

Figure 4.22: Unstable test: Current

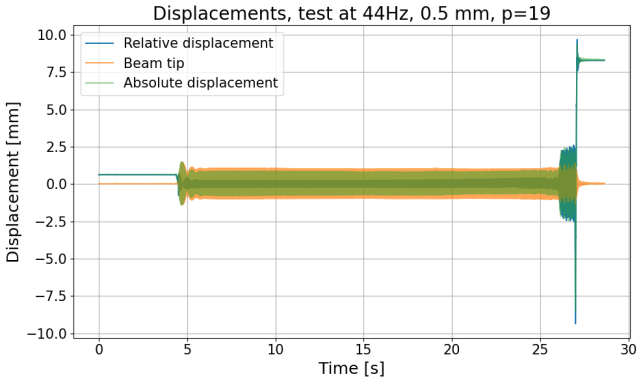

Figure 4.23: Unstable test: Displacement

4.4. Limitations

This project has been carried out with the utmost care. However, there were a few limitations in the test setup that influenced the results. These limitations should be taken into account when interpreting the results of the experiments.

The beam was clamped to a Space-frame structure. This structure was not infinitely heavy and stiff. Therefore, the vibrations in the beam would also induce vibrations in the Space-frame structure. Especially at large amplitudes of the beam vibrations, the vibrations in the Space-frame structure could become significantly apparent. The laser sensor used to measure the beam tip displacements was also attached to this Space-frame structure. Thereby, it would vibrate together with the whole structure, distorting the measurements.

In addition, the laser sensor was not perfectly in line with the displacement sensor that measured the relative cylinder displacement. The integrated displacement sensor was located inside the casing for the actuator, situated on top of the beam. The laser sensor was pointed at the beam tip, slightly below the actuator. Therefore, adding the two displacements to obtain the absolute displacement of the cylinder is not completely accurate.

The accelerometer placed on the tip of the beam was meant to serve as a back-up measurement, checking the results from the laser sensor. However, the measurements from the accelerometer contained too much noise to be useful. This was probably due to disturbances by the magnetic field of the actuator. Another measurement tool that was meant to serve as a back-up to the laser was Digital Image Correlation (DIC). Unfortunately, due to time limitations for the project in combination with the availability of the DIC camera, this was eventually not possible. Using DIC would have given an overview of the full shape of the beam, instead of only the displacement of the tip. It is a recommended measurement tool to use in future research on the actuator.

5 Model

This chapter talks about the model that was made to predict the response of the beam-actuator system. First, the structure and the development of the model are described. After that, the results and accuracy of the model are discussed.

5.1. Development

The system consists of two main parts with their own degrees of freedom, see figure 5.1. Firstly, there is the movement of the beam, denoted with a w. Secondly, there is the movement of the moving cylinder in the actuator, denoted with a u. Both parts have their own equation of motion, which are coupled through the forcing $F(t)$, see equation 5.1 and 5.2.

$$\begin{aligned} &\rho A\frac{\partial^2 w}{\partial t^2}+EI\frac{\partial^4 w}{\partial z^4}=0 \\ &at\ z=0: \quad w=0 \\ &\qquad\qquad \frac{\partial w}{\partial z}=0 \\ &at\ z=L: \quad \frac{\partial^2 w}{\partial z^2}=0 \\ &\qquad\qquad EI\frac{\partial^3 w}{\partial z^3}=m\frac{\partial^2 w}{\partial t^2}-F(t) \end{aligned} \tag{5.1}$$

$$m_a\frac{d^2u}{dt^2}=-F(t) \tag{5.2}$$

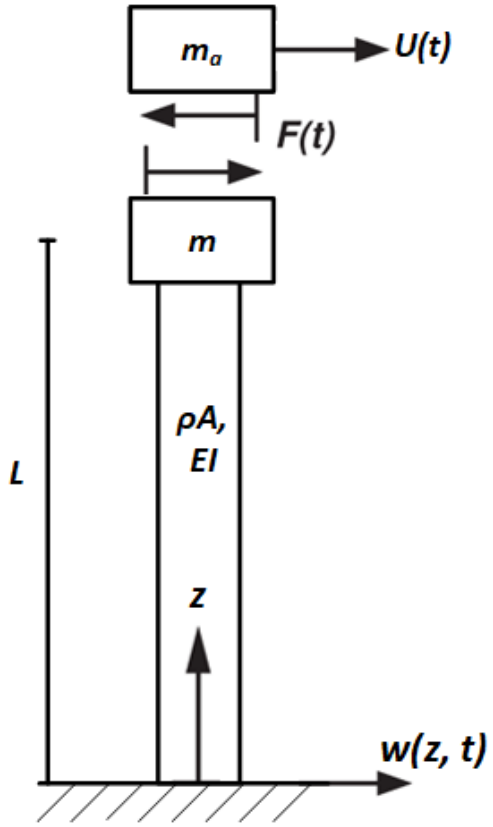

Figure 5.1: Beam-actuator system

5.1.1. From beam model to 1DOF system

The beam is modelled as an Euler-Bernoulli beam. The deflection, $w(z,t)$, is therefore determined according to the partial differential equation (PDE) 5.3. The beam-actuator system can be approximated as a cantilever beam with a tip mass, see figure 5.2. This system has boundary conditions (BC) shown in equation 5.4.

To solve the system the method of separation of variables is used. The solution is assumed to be of the form $w(z,t) = W(z) * q(t)$. This creates a separate space part, $W(z)$, and time part, $q(t)$.

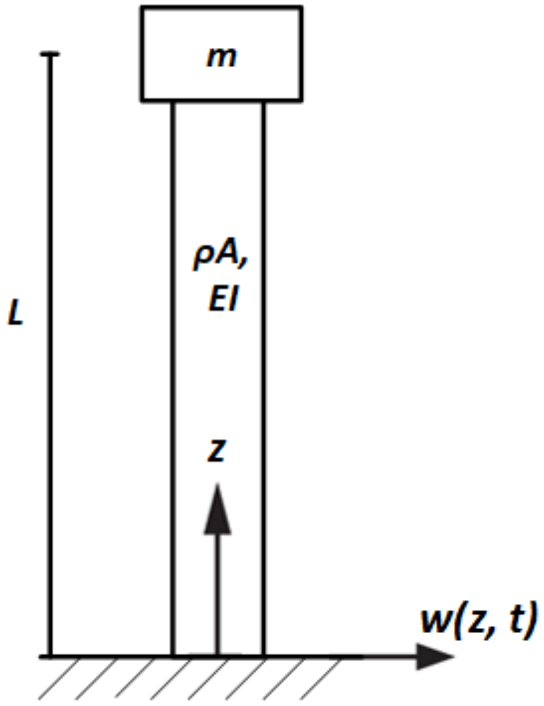

Figure 5.2: Cantilever beam with tip mass

$$\rho A \frac{\partial^2 w}{\partial t^2} + EI \frac{\partial^4 w}{\partial z^4} = 0 \tag{5.3}$$

$$\begin{aligned} at\ z = 0: \quad & w = 0 \\ & \frac{\partial w}{\partial z} = 0 \\ at\ z = L: \quad & \frac{\partial^2 w}{\partial z^2} = 0 \\ & EI \frac{\partial^3 w}{\partial z^3} = m \frac{\partial^2 w}{\partial t^2} - F(t) \end{aligned} \tag{5.4}$$

For the beam model, it is assumed that the system is vibrating at its first natural frequency, since the experiments are conducted mainly under resonance. This means that the spatial part of the beam deflection, $W(z)$, is known. It is the first mode of the system. This can be used to transform the continuous beam model to a single degree of freedom (1DOF) model in the form of a mass-spring system.

Natural frequencies

$$\begin{aligned} q(t) &= e^{i\omega t} \\ w(z,t) &= W(z) e^{i\omega t} \end{aligned} \tag{5.5}$$

To determine the mode shape, first the natural frequencies have to be calculated. In order to do this, the time-dependent part is assumed to be the harmonic function shown in equation 5.5. This is substituted into the equation of motion (EoM) and the BC. Doing this gives the ordinary differential equation (ODE) 5.6. The substituted BC can be seen in equation 5.7[1].

[1] For determining the natural frequencies, the system is considered without forcing. Therefore, the forcing term is removed from the BC.

$$-\rho A\omega^2 W + EI\frac{\partial^4 W}{\partial z^4} = 0 \tag{5.6}$$

$$\begin{aligned} at\ z = 0: \quad & W = 0 \\ & \frac{\partial W}{\partial z} = 0 \\ at\ z = L: \quad & \frac{\partial^2 W}{\partial z^2} = 0 \\ & EI\frac{\partial^3 W}{\partial z^3} + m\omega^2 W = 0 \end{aligned} \tag{5.7}$$

The general solution of the ODE has four unknown constants and can be seen in equation 5.8. The general solution is substituted into the BC in equation 5.7. This results in a system of four equations, the boundary conditions, and four unknowns, the constants. This system can be represented in matrix form as shown in equation 5.9. The natural frequencies of the system can be found with the help of this matrix.

$$W(z) = C_1 e^{-z\left(\frac{A\omega^2\rho}{EI}\right)^{\frac{1}{4}}} + C_2 e^{z\left(\frac{A\omega^2\rho}{EI}\right)^{\frac{1}{4}}} + C_3 e^{-iz\left(\frac{A\omega^2\rho}{EI}\right)^{\frac{1}{4}}} + C_4 e^{iz\left(\frac{A\omega^2\rho}{EI}\right)^{\frac{1}{4}}} \tag{5.8}$$

$$\begin{bmatrix} 1 & 1 & 1 & 1 \\ -\left(\frac{A\omega^2\rho}{EI}\right)^{\frac{1}{4}} & \left(\frac{A\omega^2\rho}{EI}\right)^{\frac{1}{4}} & -i\left(\frac{A\omega^2\rho}{EI}\right)^{\frac{1}{4}} & i\left(\frac{A\omega^2\rho}{EI}\right)^{\frac{1}{4}} \\ \sqrt{\frac{A\omega^2\rho}{EI}}e^{-L\left(\frac{A\omega^2\rho}{EI}\right)^{\frac{1}{4}}} & \sqrt{\frac{A\omega^2\rho}{EI}}e^{L\left(\frac{A\omega^2\rho}{EI}\right)^{\frac{1}{4}}} & -\sqrt{\frac{A\omega^2\rho}{EI}}e^{-iL\left(\frac{A\omega^2\rho}{EI}\right)^{\frac{1}{4}}} & -\sqrt{\frac{A\omega^2\rho}{EI}}e^{iL\left(\frac{A\omega^2\rho}{EI}\right)^{\frac{1}{4}}} \\ -EI\left(\frac{A\omega^2\rho}{EI}\right)^{\frac{3}{4}}e^{-L\left(\frac{A\omega^2\rho}{EI}\right)^{\frac{1}{4}}} + m\omega^2 e^{-L\left(\frac{A\omega^2\rho}{EI}\right)^{\frac{1}{4}}} & EI\left(\frac{A\omega^2\rho}{EI}\right)^{\frac{3}{4}}e^{L\left(\frac{A\omega^2\rho}{EI}\right)^{\frac{1}{4}}} + m\omega^2 e^{L\left(\frac{A\omega^2\rho}{EI}\right)^{\frac{1}{4}}} & iEI\left(\frac{A\omega^2\rho}{EI}\right)^{\frac{3}{4}}e^{-iL\left(\frac{A\omega^2\rho}{EI}\right)^{\frac{1}{4}}} + m\omega^2 e^{-iL\left(\frac{A\omega^2\rho}{EI}\right)^{\frac{1}{4}}} & -iEI\left(\frac{A\omega^2\rho}{EI}\right)^{\frac{3}{4}}e^{iL\left(\frac{A\omega^2\rho}{EI}\right)^{\frac{1}{4}}} + m\omega^2 e^{iL\left(\frac{A\omega^2\rho}{EI}\right)^{\frac{1}{4}}} \end{bmatrix} \begin{bmatrix} C1 \\ C2 \\ C3 \\ C4 \end{bmatrix} = \begin{bmatrix} 0 \\ 0 \\ 0 \\ 0 \end{bmatrix} \tag{5.9}$$

All the parameters in this matrix are known except for one, the frequency ω. The natural frequencies are those frequencies that make the determinant of the matrix equal to zero. By first substituting all the known values for the other parameters and then setting the determinant to zero, the natural frequencies can be determined.

Mode shapes

With the natural frequencies known, the mode shapes can be determined. They are derived from the general solution shown in equation 5.8. The only unknowns in this solution are the four constants. They are determined using the system of equations in 5.9. However, not all four constants can be determined through this system. At the natural frequencies, the determinant of the matrix is zero. This results in one of the rows being a linear combination of the other three. Therefore, only three independent equations remain and only three of the four unknowns can be calculated.

This problem is avoided by assuming C_4 to have a value of 1. This leaves only three unknowns, which can be solved with the three independent equations in 5.9. Substituting the three solved constants back into equation 5.8 gives the mode shape. This mode shape is then normalized to have a tip deflection of one. By doing this the deflection of the mass-spring system will match the deflection of the tip of the beam. The normalized first mode shape of the system can be seen in figure 5.3.

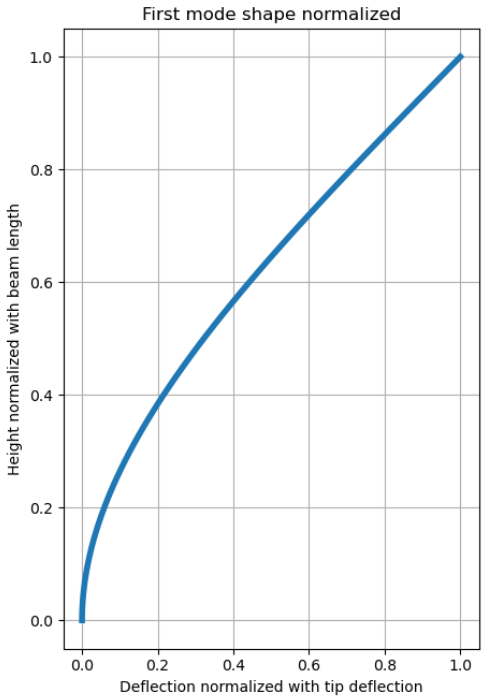

Figure 5.3: First mode shape

Mass-spring system

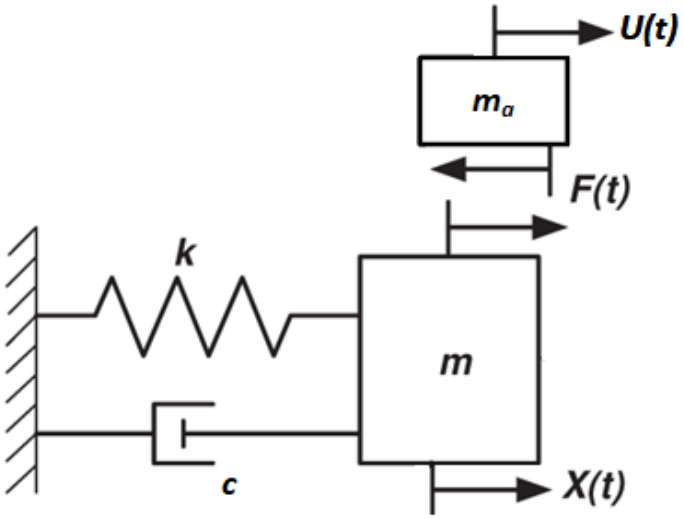

Figure 5.4: Mass-spring-dashpot-actuator system

To set up the mass-spring system as shown in figure 5.4, the correct values for the parameters[2] need to be determined. These turn out to be the modal quantities and can be calculated using equation 5.10. A derivation of these formulas can be found in appendix A.

[2]The parameters are: the spring stiffness k, the damping coefficient c, the mass m and the force F(t).

The mass, spring stiffness and forcing[3] are calculated based on the mode shape of the beam, using equation 5.10. Since the mode shape is normalised to have a tip deflection of 1, the modal force is equal to the physical force from the actuator. Damping is added to the system as modal damping for the beam. The damping ratio first has to be assumed. It is later tuned based on the results from the physical experiments[4]. The modal damping can be calculated using equation 5.11. A derivation of this formula can be found in appendix A. In addition to damping in the beam, a damping term is also added to the equation of motion for the actuator, C_{act}.

$$\begin{aligned} M_m &= \int_0^L W_n \rho A W_n \, dz \\ K_m &= \int_0^L W_n EI \frac{\partial^4 W_n}{\partial z^4} \, dz \\ F_m(t) &= W_n(L) F(t) = 1 * F(t) \end{aligned} \tag{5.10}$$

$$C_m = 2\zeta\sqrt{M_m K_m} \tag{5.11}$$

The system in figure 5.4 has two EoM's: one for the movement of mass m, shown in equation 5.12, and one for the movement of mass m_a, shown in equation 5.13.

$$M_m \frac{d^2x}{dt^2} + C_m \frac{dx}{dt} + K_m x = F(t) \tag{5.12}$$

$$M_a \frac{d^2u}{dt^2} + C_{act} \frac{du}{dt} = -F(t) \tag{5.13}$$

Forcing

In real life, the input for the actuator is the current $I(t)$, resulting in the electromagnetic force $F(t)$. The precise theoretical modelling of the working of the actuator is beyond the scope of this project. Therefore, the current and the force are assumed to be related through a parameter A, see equation 5.14. The value of this parameter is determined based on previous tests performed with the actuator and is found to be frequency dependent (Follet and Weening, 2024). An overview of the values of parameter A can be found in appendix B. Substituting equation 5.14 into the EoM's gives equation 5.15

$$F(t) = A * I(t) \tag{5.14}$$

$$\begin{aligned} M_m \frac{d^2x}{dt^2} + C_m \frac{dx}{dt} + K_m x &= A * I(t) \\ M_a \frac{d^2u}{dt^2} + C_{act} \frac{du}{dt} &= -A * I(t) \end{aligned} \tag{5.15}$$

5.1.2. State-space system

To solve the two equations, a state-space system is introduced. Four new variables are introduced to replace the variables x and u, as shown in equation 5.16. These new variables are substituted into the EoM's, see equation 5.17.

$$\begin{aligned} x_1 &= x \\ x_2 &= \frac{dx}{dt} \\ x_3 &= u \\ x_4 &= \frac{du}{dt} \end{aligned} \tag{5.16}$$

[3] $F(t)$ is the physical force acting at the tip of the beam. $F_m(t)$ is the modal force that is used in the mass-spring system.
[4] The damping ratio is tuned to be 1.8%, meaning that the modal damping is 1.8% of the critical damping.

$$\begin{aligned} M_m \frac{dx_2}{dt} + C_m x_2 + K_m x_1 &= A * I(t) \\ M_a \frac{dx_4}{dt} + C_{act} x_4 &= -A * I(t) \end{aligned} \tag{5.17}$$

The EoM's in equation 5.17 can be rewritten into formulas for the first derivatives of the four variables, giving equation 5.18. These four equations can also be written in matrix form, resulting in equation 5.19.

$$\begin{aligned} \frac{dx_1}{dt} &= x_2 \\ \frac{dx_2}{dt} &= (-K_m x_1 - C_m x_2 + AI)/M_m \\ \frac{dx_3}{dt} &= x_4 \\ \frac{dx_4}{dt} &= (-C_{act} x_4 - AI)/M_a \end{aligned} \tag{5.18}$$

$$\begin{bmatrix} \frac{dx_1}{dt} \\ \frac{dx_2}{dt} \\ \frac{dx_3}{dt} \\ \frac{dx_4}{dt} \end{bmatrix} = \begin{bmatrix} 0 & 1 & 0 & 0 \\ -K_m/M_m & -C_m/M_m & 0 & 0 \\ 0 & 0 & 0 & 1 \\ 0 & 0 & 0 & -C_{act}/M_a \end{bmatrix} \begin{bmatrix} x_1 \\ x_2 \\ x_3 \\ x_4 \end{bmatrix} + \begin{bmatrix} 0 \\ A/M_m \\ 0 \\ -A/M_a \end{bmatrix} I \tag{5.19}$$

5.1.3. Control setting

The actuator can be used via two different control settings, open-loop and closed-loop. These two setting require slightly different computer models to accurately describe their behaviour and predict the response of the system.

Closed-loop

In the closed-loop setting, the actuator uses a PID controller to perform position control on the relative motion between the actuator and the beam tip. This relative motion can be deduced from system 5.19 by subtracting x_1 from x_3, see equation 5.20. The controller uses a sinusoidal input signal, u_{set} that the relative motion should follow, see equation 5.21. The amplitude and frequency of the signal can be set to the desired values. The difference between u_{set} and the actual motion, u_a is called the error, see equation 5.22. The PID controller uses this error to determine the input current that has to be sent to the actuator, equation 5.23. The three parameters in this control function have to be tuned manually until the output u_a matches the input signal u_{set}.

$$u_a(t) = x_3 - x_1 \tag{5.20}$$

$$u_{set}(t) = ampl * sin(\Omega t) \quad [5] \tag{5.21}$$

$$e(t) = u_{set}(t) - u_a(t) \tag{5.22}$$

$$I(t) = K_p * e(t) + \int_0^t K_i e(\tau) d\tau + K_d \frac{de(t)}{dt} \tag{5.23}$$

Open-loop

In the open-loop setting, the current that is sent to the actuator is directly controlled. The input signal u_{set} now corresponds to the desired current. The current, I in system 5.19, can be set equal to the control signal u_{set}. The system can then be run to determine the response of the system.

[5] Note that the unit of the amplitude for the control signal depends on the control setting, mm for closed-loop and A for open-loop.

5.2. Results

Frequency sweeps are performed using the computer model. The graphs created by these sweeps can be compared with the graphs from the real-life tests, to analyse the accuracy of the model.

5.2.1. Open-loop

Figure 5.5 shows the plot for the beam tip displacement in the computer model, compared to the physical experiments. It follows a similar pattern to the graph from the real-life experiments, with a peak at the same frequency. However, the magnitude of the graph differs between the model and the experiments. The model shows higher values than the experiments. This can have multiple causes, as the model has a few imperfections.

First of all the beam is modelled to be perfectly clamped at the bottom. In reality the clamp is probably not fully rigid, but acts more as a rotational spring. This, among other imperfections in the model, caused the natural frequency of the model to be higher than in real-life, 64 Hz instead of 47 Hz. Results from the model with a beam length of 1 m can be found in appendix D The beam length in the model was increased from 1 m to 1.2 m. In addition to the clamp, this also compensated for an inaccuracy in the modelling of the actuator. The actuator was modelled as a tip mass with no volume. In reality, it does have a volume. Therefore, the centre of mass of the actuator is not located at the tip of the beam, but 6.5 cm above. The longer beam length partly compensates for this extra distance. Increasing the beam length resulted in correct natural frequencies in the model, both for the actuator in operation, 47 Hz, and for the actuator not in operation, 43.5 Hz. However, this increased beam length might result in larger tip deflections.

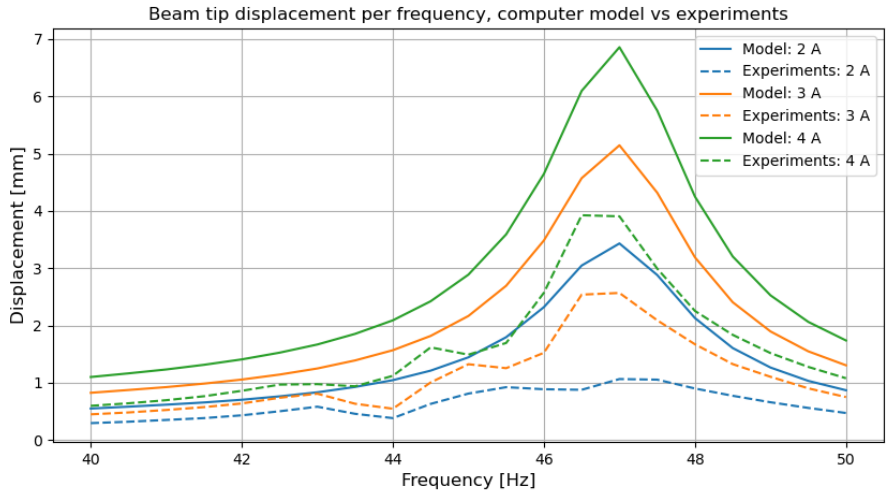

Figure 5.5: Model vs experiments for open-loop: Beam tip displacement

In addition, the model does not take into account the Back EMF. This Back EMF causes the current to be lower at the resonance frequency, see figure 5.6. Since the model has no Back EMF, the current at resonance is higher than in real-life, resulting in larger beam tip deflections.
Figure 5.7 shows the beam tip displacement, normalised by the current in the actuator. In this plot, the graph for the model is closer to the experiment results. The model follows the curve of the experiments fairly well, only slightly shifted upwards.

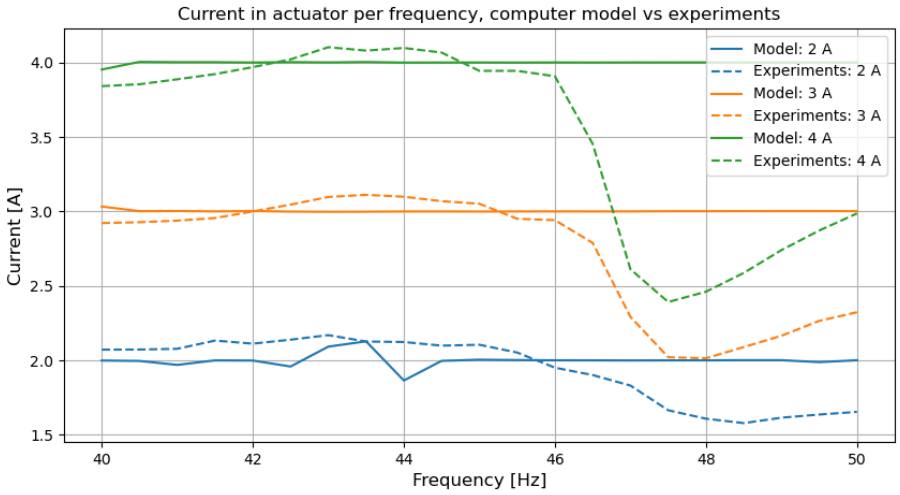

Figure 5.6: Model vs experiments for open-loop: Current in actuator

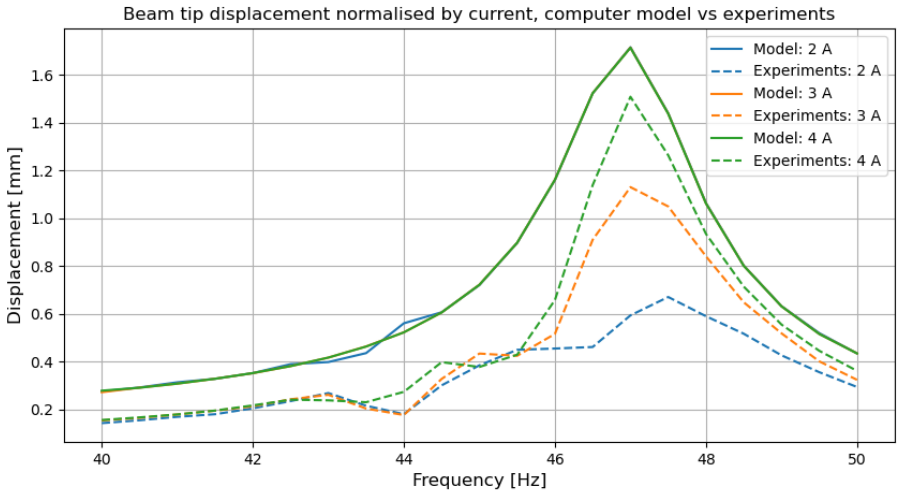

Figure 5.7: Model vs experiments for open-loop: Normalised beam tip displacement

Another large influence for the results of the model is damping. The damping ratio used in the model was tuned to have the results of the model match the real-life experiments as good as possible. This was done based on the graph in figure 5.7 and on the phase difference between the beam tip displacement and the cylinder displacement, see figure 5.8. The phase difference of the model and the experiments both show a shift from 0 degrees to 180 degrees. The steepness of this shift depends on the damping in the system and was used to tune the damping in the model. The damping ratio used to create the results in this chapter was 1.8%.

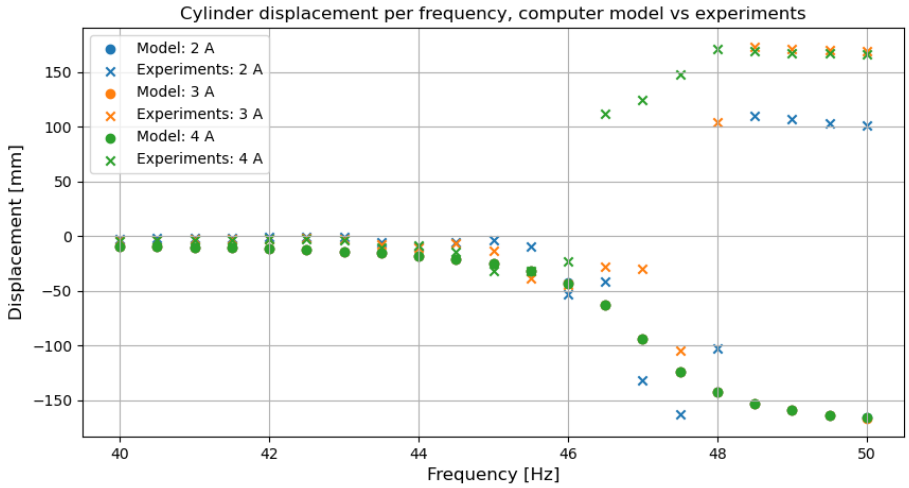

Figure 5.8: Model vs experiments for open-loop: Phase shift

5.2.2. Closed-loop

For the closed-loop setting, the computer model is executed multiple times. First, the model is run controlling the relative displacement of the cylinder. The results of this simulation are compared to the results from the experiments. In addition, the model is set to control the absolute motion of the cylinder. Finally, it is also set to control the beam tip displacement. The latter two settings were not possible in the real-life experiments, due to limitations of the test setup. However, the results of the computer model can be used to determine whether this would be useful to explore in future physical experiments.

Controlling relative motion

The computer model performs slightly less well in predicting the response of the system for the closed-loop setting than for the open-loop setting. The graphs show patterns similar to the results from the experiments[6]. However, the graph seems to be shifted to the left. The frequency at which the locking effect is most present has moved, from 43.5 Hz in the experiments to 40 Hz in the computer model. This is remarkable, considering that this does not coincide with the natural frequency of the model. If the mass of the moving cylinder is added to the tip mass, the model has a natural frequency of 43.5 Hz. This matches the frequency of the physical system found in the hammer tests, see chapter 4.1.

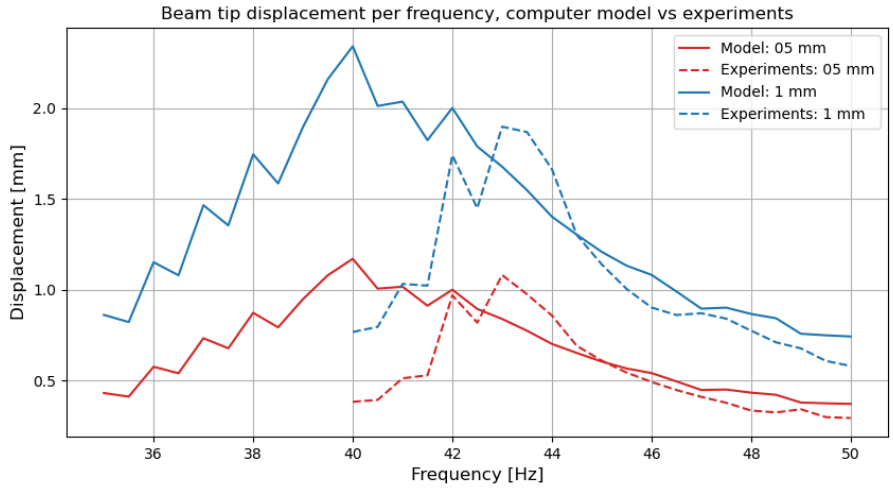

Figure 5.9: Model vs experiments for closed-loop: Beam tip displacement

[6]For the computer model, the frequency sweeps were performed over a longer range than in the experiments, 35-50 Hz instead of 40-50 Hz. This was done in order to fully show the peak from the locking effect.

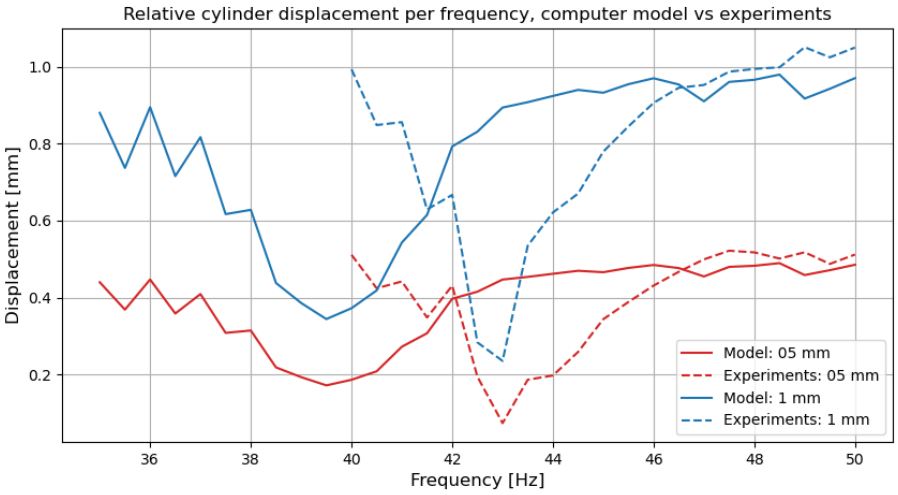

Figure 5.10: Model vs experiments for closed-loop: Relative cylinder displacement

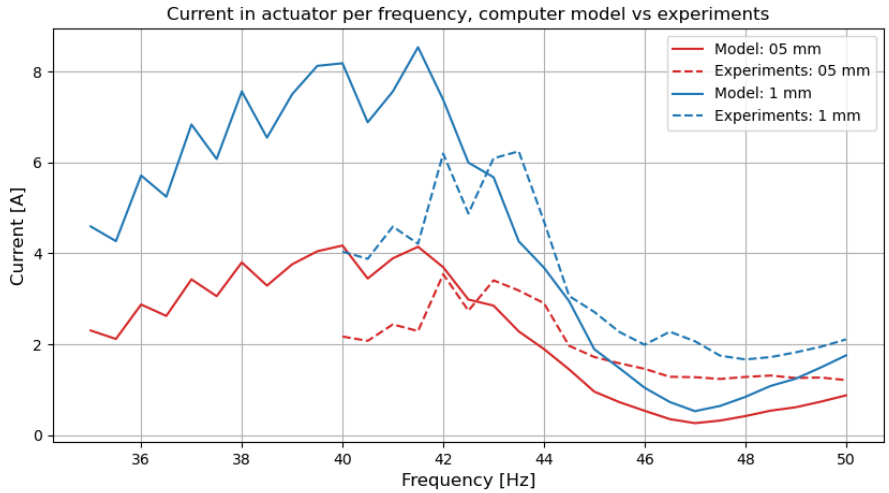

Figure 5.11: Model vs experiments for closed-loop: Current in actuator

Another difference between the model and the experiments is visible in figure 5.12. The model shows a large peak for the normalised beam tip displacement at 47 Hz, which is not present in the results from the experiments. The reason for this is that the model underestimates the needed current at that frequency, see figure 5.11. At 47 Hz, a small current can induce large relative displacements of the cylinder, since it is the resonance frequency. However, to ensure a smooth harmonic motion of the relative displacement, in real-life a less smooth harmonic current signal with a larger amplitude is needed. The computer model, on the other hand, creates a harmonic displacement signal with a small harmonic current signal. See appendix C for the comparison between the time series.

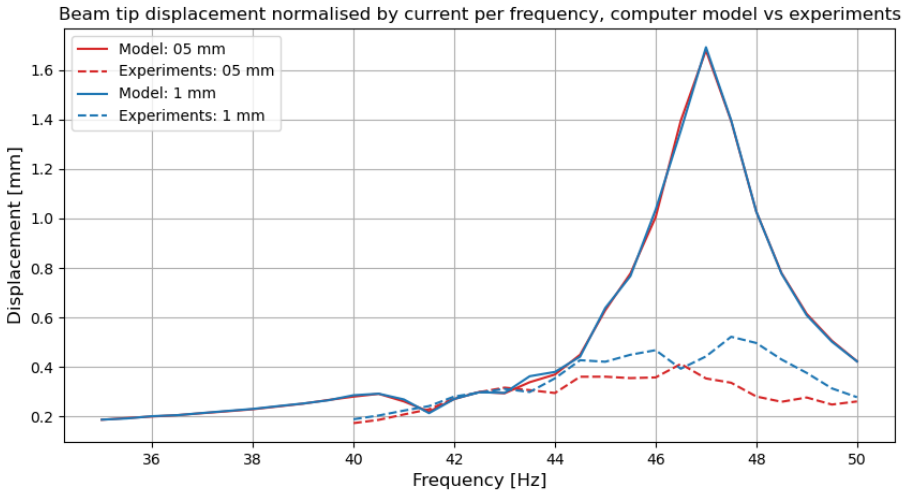

Figure 5.12: Model vs experiments for closed-loop: Normalised beam tip displacement

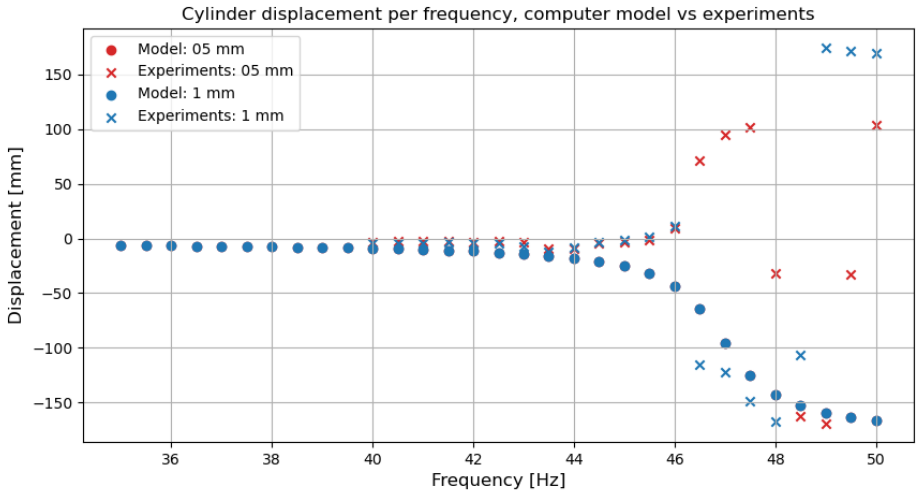

Figure 5.13: Model vs experiments for closed-loop: Phase shift

Controlling absolute motion

The results of the computer model controlling the absolute motion of the cylinder are promising. Figure 5.14 shows that resonance at 47 Hz can be induced by controlling the absolute motion of the cylinder. The absence of this resonance was a large disadvantage of controlling the relative displacement. In addition, the physical experiments showed that using a closed-loop setting gave better predictability of the beam tip displacement than using the open-loop setting, see chapter 4.2.5. Therefore, controlling the absolute motion of the cylinder could take the best of both methods, inducing large displacements at resonance with higher predictability.

However, these results should be interpreted with care. The model has shown to sometimes overestimate the response of the system, see figures 5.5 and 5.12. The relative cylinder displacements are large at resonance, see figure 5.17. Therefore, Back EMF will most likely play a significant role in the response of the system, which is not accounted for in this computer model. In order to determine whether this control setting would be a viable and useful option, more research with physical experiments would be needed, to check the efficiency and predictability of the system.

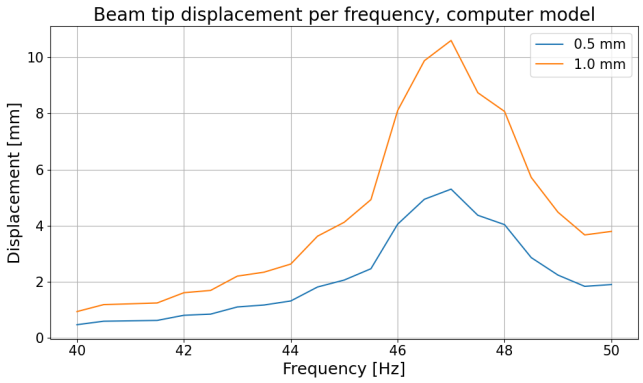

Figure 5.14: Model controlling u_{abs}: Beam tip displacement

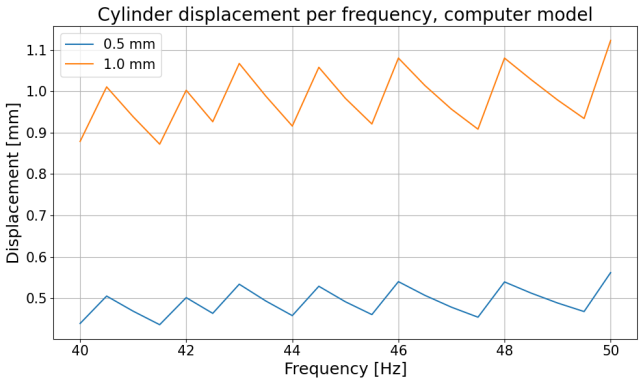

Figure 5.15: Model controlling u_{abs}: Absolute cylinder displacement

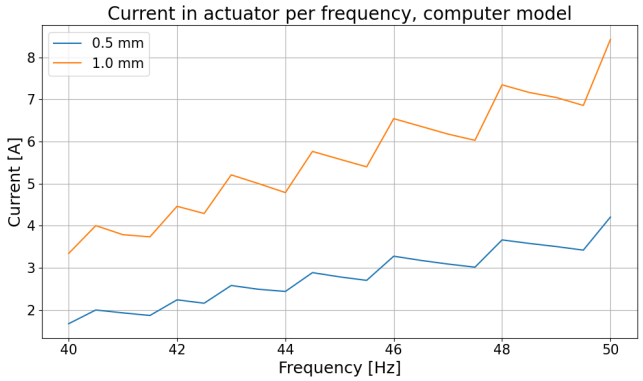

Figure 5.16: Model controlling u_{abs}: Current in actuator

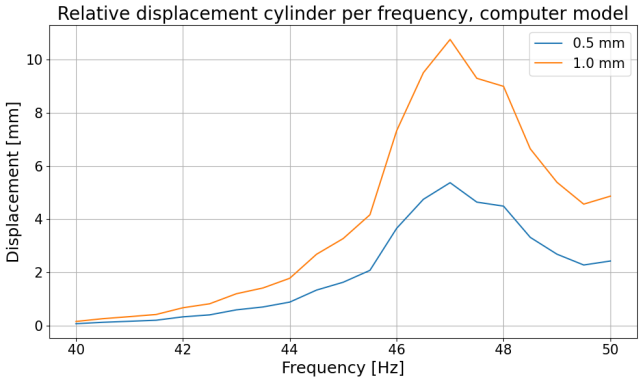

Figure 5.17: Model controlling u_{abs}: Relative cylinder displacement

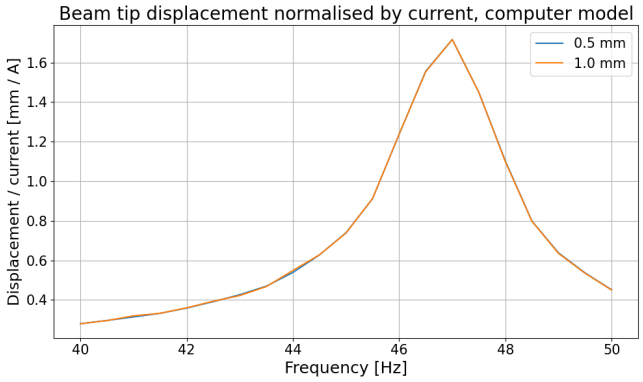

Figure 5.18: Model controlling u_{abs}: Normalised beam tip displacement

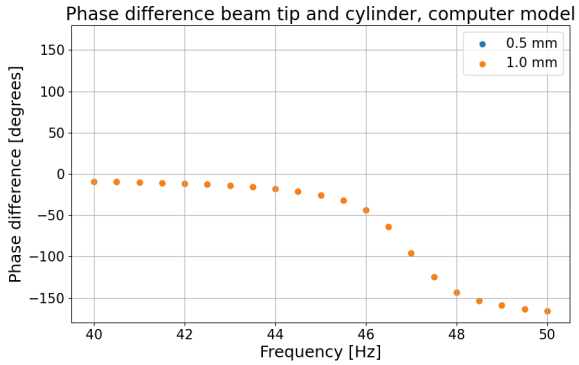

Figure 5.19: Model controlling u_{abs}: Phase shift

Controlling beam tip

Controlling the beam tip displacement could also be a useful control setting to use on the actuator. In this way, the output would be controlled most directly. Figures 5.20 through 5.25 show the results of the computer model using this setting. The current in the actuator drops significantly around the resonance frequency. The beam tip displacement stays constant, as it is the variable that is being controlled, see figure 5.20. This results in a high efficiency, see figure 5.24. However, similar peaks in efficiency were visible in the model when controlling the relative cylinder motion. This peak was significantly smaller

in the physical experiments, see figure 5.12. Therefore, more research with physical experiments are recommended. These experiments can check the efficiency and predictability of the system at this setting and determine if it is a useful control setting for the actuator.

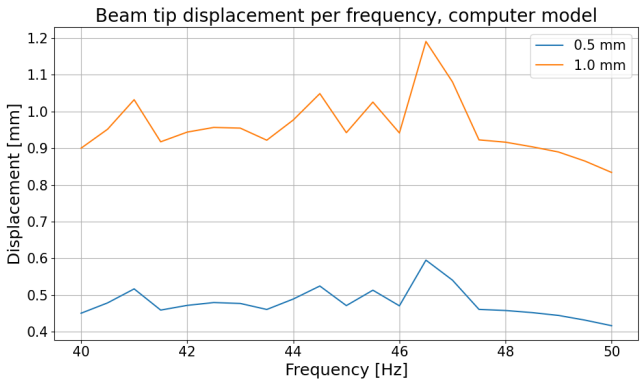

Figure 5.20: Model controlling beam: Beam tip displacement

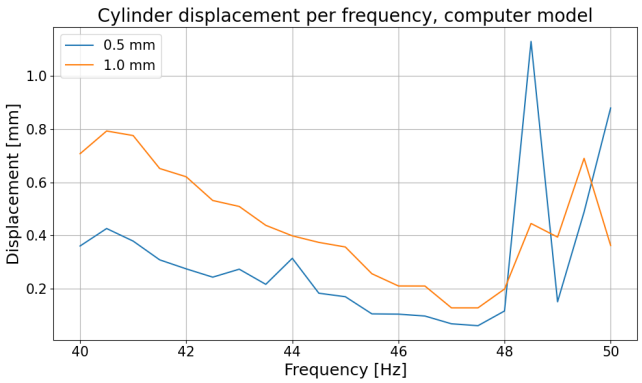

Figure 5.21: Model controlling beam: Absolute cylinder displacement

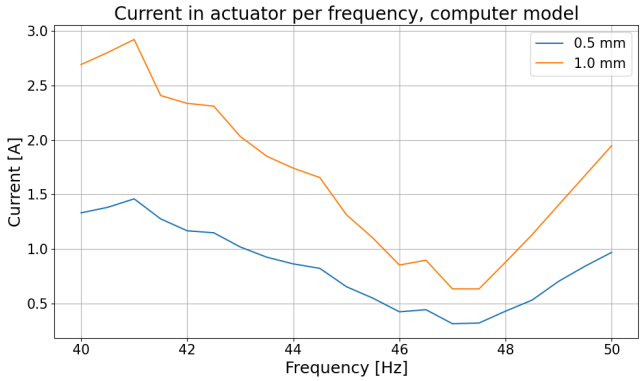

Figure 5.22: Model controlling beam: Current in actuator

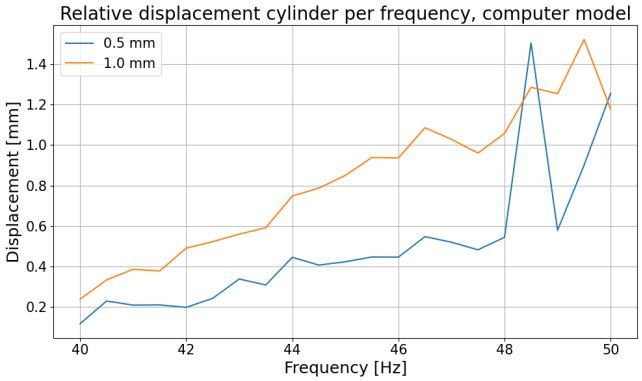

Figure 5.23: Model controlling beam: Relative cylinder displacement

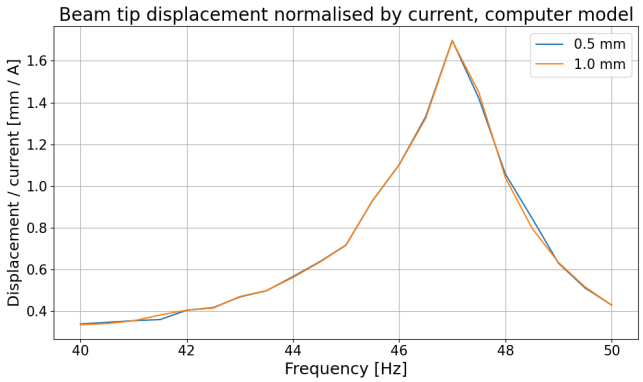

Figure 5.24: Model controlling beam: Normalised beam tip displacement

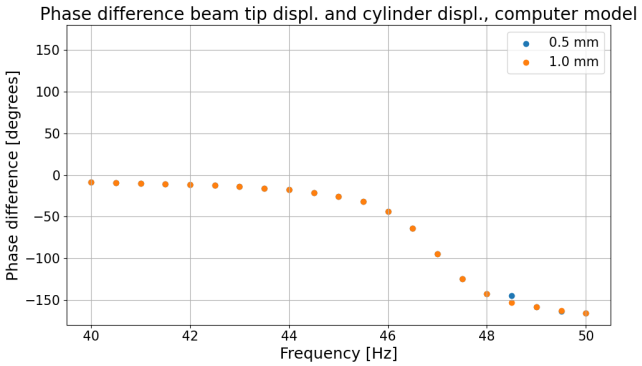

Figure 5.25: Model controlling beam: Phase shift

6

Conclusions and recommendations

This chapter gives the conclusions of the project by answering the research questions. In addition, some recommendations are made for future use of and research into the actuator.

6.1. Research questions

Answering the main research question:
"How does the coupled dynamic behaviour between an electromagnetic actuator and a flexible beam influence its performance?"

The manner in which the dynamic behaviour of the beam and the actuator interact with each other depends on the input setting. However, for both settings, they counteract each other a little.

The beam vibrates most efficiently at its resonance frequency. However, for the open-loop setting, at this frequency the relative displacements between cylinder and beam become really large, resulting in a large back-emf and therefore larger voltage needed. This results in a larger amount of electrical power being used and thereby largely negates the efficiency of the resonance.

In the closed loop setting, the control mechanism of the actuator kills the resonance in the system, by limiting the relative displacement of the cylinder.

Answering the sub-questions:

- *"How can instabilities in the system be prevented?"*
    - In general, instabilities can be prevented by not pushing the actuator too hard to its limits. The exact ways instabilities can occur depend on the control setting used.

      The closed loop setting is the most prone to instabilities. The amplitude of vibration can suddenly and rapidly increase when the parameters for the PID controller are not tuned correctly. Especially if the P-value is too high, these instabilities are likely to occur. Therefore, the parameters must be tuned with caution. If necessary, a small safety margin for the P-value should be used.

      The open loop setting is less prone to instabilities. If the input current is maintained within the limits given by the manufacturer, the actuator can be safely used.
- *"To what extent does the Sommerfeld effect play a role in the beam-actuator interaction?"*
    - The Sommerfeld effect plays a very small role in the beam-actuator interaction. The Sommerfeld effect mostly occurs when using rotating motors. In these motors, only the speed of the motor can be adjusted. For the linear motor used in this thesis, both the amplitude and frequency of the motor can separately be adjusted. The system was always able to vibrate at the input frequency and did not show signs of resonance locking.

- *"What elements does a numerical model need to have to be able to accurately predict the response of the beam?"*
    - The computer model created for this thesis is reasonably capable of predicting the system's response. The output of the model matches the results of the real-life tests in terms of amplitude and phase for most input settings. However, there are some elements that could be added to the model to make it more robust and accurate for all inputs.

      One of the most important elements that should be added is Back EMF. In the physical experiments, Back EMF played a large role in the working of the actuator. Incorporating the Back EMF into the computer model is expected to significantly improve the accuracy of its results.

      In addition, the beam-actuator system could be modelled to be more physically accurate. The clamp at the bottom of the beam could be changed from a perfect clamp to a rotational spring. The physical properties of the actuator are also simplified in the current model. It is modelled as a point mass, while in reality it is a rigid body with rotational inertia.

      The model uses the linear Euler-Bernoulli equation for the beam. This part of the model could be changed to be able to account for non-linear displacements. However, given the current performance of the model, this is not expected to lead to a large increase in its accuracy.
- *"Which input settings on the actuator result in the best performance?"*
    - There is no ideal control setting for the actuator. Each setting has its advantages and disadvantages. Therefore, the best setting to choose depends on the situation. For this thesis, effectiveness is prioritised over the other criteria. The resulting best input setting is applying a large current signal at 47 Hz in the open-loop setting, followed closely by using the closed-loop setting at 47 Hz.

      As discussed in chapter 5.2.2, the results of the computer model controlling the beam motion and the absolute motion of the cylinder looked promising. These settings could combine high scores for both effectiveness and predictability. Future research with physical experiments on these settings is recommended.

6.2. Recommendations for future use

Shortening beam length

During the installation of the monopile, the length of the pile above the ground decreases. This shorter length results in smaller displacements at the tip of the pile. It is important to take this into account when using closed-loop position controlling for the actuator. Sustaining the same amplitude could require significantly more input power at smaller beam lengths than at longer beam lengths.

Resonance

The most effective way to use the actuator is by putting the system into resonance. However, in real life applications, the natural frequency of the system may be unknown. In addition, the natural frequency will change when installing the monopile, as the portion of the pile above the ground decreases. The shorter remaining pile length results in a larger natural frequency.

To find the initial natural frequency, a simple impact test can be used. The installation of the pile can then be started with this frequency as the operating frequency. During the installation, this operating frequency has to be adjusted to keep the system in resonance. This can be done by keeping track of a variable that would change when system goes out of resonance. When the value of that variable changes, the operating frequency has to be increased.

The best variable to keep track of depends on the control setting that is being used. When using the open-loop setting, the voltage across the actuator can be used. Due to the Back EMF, resonance coincides with a large voltage. Therefore, a decreasing voltage indicates that the system is going out of resonance. The beam tip displacement is a variable that could also be used, with a decreasing displacement indicating that the system is going out of resonance. However, this should be interpreted with care, as the shorter beam length in itself also results in smaller tip displacements.

For closed-loop settings, further research with physical experiments has to show if Back EMF plays a role when controlling either the beam tip displacement or the absolute motion of the cylinder. If it plays a role, this could be used to keep track of the resonance in the system.

References

Actuonix Motion Devices. (2024, October 1). *How do electric actuators work?* https://www.actuonix.com/how-do-electric-actuators-work-?srsltid=AfmBOooz1XrVBPs1hkzDQ5-BP-sFRz0l0lyKHZi5cZmgDGrj3OObkKL1

American Clean Power. (2025). offshore-wind-turbines-sunrise-1. https://cleanpower.org/facts/offshore-wind/

Barari, A., Dadashpour Kaliji, H., Ghadimi, M., & domiri ganji, D. (2011). Non-linear vibration of euler-bernoulli beams. *Latin American Journal of Solids and Structures*, *8*, 139–148. https://doi.org/10.1590/S1679-78252011000200002

Chen, X., Zhou, B., Zhang, J., & Liu, J. (2024). Experiments on sommerfeld effect in a non-ideal vibration system driven by ac motor. *Journal of the Brazilian Society of Mechanical Sciences and Engineering*, *46*(1), 7.

Das, D., Sahoo, P., & Saha, K. (2012). A numerical analysis of large amplitude beam vibration under different boundary conditions and excitation patterns. *Journal of Vibration and Control*, *18*, 1900–1915. https://doi.org/10.1177/1077546311429147

Du, H., Chau, F., & Zhou, G. (2018). Harmonically-driven snapping of a micromachined bistable mechanism with ultra-small actuation stroke. *Journal of Microelectromechanical Systems*, *PP*, 1–6. https://doi.org/10.1109/JMEMS.2017.2785331

Duff-Norton. (2022, December 20). *Hydraulic vs. electric linear actuator: Which is best?* https://www.cmco.com/en-us/resources/duff-norton-blogs/choosing-between-hydraulic-and-electric-linear-actuators/

Felix, J. L. P., Balthazar, J. M., & Brasil, R. (2009). Comments on nonlinear dynamics of a non-ideal duffing-rayleigh oscillator: Numerical and analytical approaches. *Journal of Sound and Vibration*, *319*(3), 1136–1149. https://doi.org/https://doi.org/10.1016/j.jsv.2008.06.036

Follet, G., & Weening, S. (2024, November). *Characterization Electromagnetic Actuator: A GDP subproject* (tech. rep.). TU Delft.

Gonçalves, P., Silveira, M., Pontes Junior, B., & Balthazar, J. (2014). The dynamic behavior of a cantilever beam coupled to a non-ideal unbalanced motor through numerical and experimental analysis. *Journal of Sound and Vibration*, *333*(20), 5115–5129. https://doi.org/https://doi.org/10.1016/j.jsv.2014.05.039

Heerema Marine Contractors. (2024, November 5). *Heerema installs monopile foundations at he dreiht*. Retrieved December 18, 2024, from https://vimeo.com/1026440882/2539f7b18c

Instrumentation Tools. (2024). *What is a hydraulic actuator ?* https://instrumentationtools.com/what-is-a-hydraulic-actuator/

Jongen, R. (2025). *Monopiles & Transition Pieces*. https://sif-group.com/en/monopiles-and-transition-pieces/

Magnetic Innovations. (n.d.). MMB 9054. https://www.magneticinnovations.com/nl/producten/lineaire-actuator/mmb-9054/?_gl=1*2sswkt*_up*MQ..*_ga*MzA1NDEyOTcuMTc1NzMyOTQ4OA..*_ga_5G2CKNRS8X*czE3NTczMjk0ODckbzEkZzEkdDE3NTczMjk1MDUkajQyJGwwJGgw

Metrikine, A. (2022, February). *Gentle Driving of Piles (GDP)*. https://grow-offshorewind.nl/project/gentle-driving-of-piles

Nierstrasz, D. (2023, October). Gentle Driving of Piles 2.0 (GDP2.0). https://grow-offshorewind.nl/project/gdp2-0

Öchsner, A. (2021, June). *Classical Beam Theories of Structural Mechanics* (1st ed.). Springer Cham. https://doi.org/10.1007/978-3-030-76035-9

Roncen, T., Sinou, J.-J., & Lambelin, J.-P. (2018). Non-linear vibrations of a beam with non-ideal boundary conditions and uncertainties – modeling, numerical simulations and experiments. *Mechanical Systems and Signal Processing*, *110*, 165–179. https://doi.org/https://doi.org/10.1016/j.ymssp.2018.03.013

Tari, H. (2013). On the parametric large deflection study of euler–bernoulli cantilever beams subjected to combined tip point loading. *International Journal of Non-Linear Mechanics*, *49*, 90–99. https://doi.org/https://doi.org/10.1016/j.ijnonlinmec.2012.09.004

Tougaard, J., & Mikaelsen, M. (2024). Underwater noise from pile driving: Comparison of german and danish regulatory frameworks.

Wang, X., Zeng, X., Li, J., Yang, X., & Wang, H. (2018). A review on recent advancements of substructures for offshore wind turbines. *Energy Conversion and Management*, *158*, 103–119. https://doi.org/https://doi.org/10.1016/j.enconman.2017.12.061

Weeger, O., Wever, U., & Simeon, B. (2013). Isogeometric analysis of nonlinear euler–bernoulli beam vibrations. *Nonlinear Dynamics*, *72*, 813–835.

Wei, H., Pan, Q., Adetoro, O., Avital, E., Yuan, Y., & Wen, P. (2020). Dynamic large deformation analysis of a cantilever beam. *Mathematics and Computers in Simulation*, *174*, 183–204. https://doi.org/https://doi.org/10.1016/j.matcom.2020.02.022

Zhang, X., Li, Z., Li, M., & Wen, B. (2021). Stability and sommerfeld effect of a vibrating system with two vibrators driven separately by induction motors. *IEEE/ASME Transactions on Mechatronics*, *26*(2), 807–817. https://doi.org/10.1109/TMECH.2020.3003029

A

Formula derivations

This appendix shows derivations of formulas used in this report.

A.1. Modal mass, damping, stiffness and forcing

The modal quantities are derived from the equation of motion, A.1. For the derivation of the modal forcing, the forcing at the tip of the beam is added to the equation of motion with the help of a Dirac Delta function. Substituting the assumed separation of variables, equation A.2, into the equation of motion gives equation A.3.

$$\rho A \frac{\partial^2 w}{\partial t^2} + c\frac{\partial w}{\partial t} + EI\frac{\partial^4 w}{\partial z^4} = \delta(z-L)F(t) \tag{A.1}$$

$$w(z,t) = \sum_{m=1}^{\infty} W_m(z) q_m(t) \tag{A.2}$$

$$\rho A \sum_{m=1}^{\infty} W_m \frac{\partial^2 q_m}{\partial t^2} + c\sum_{m=1}^{\infty} W_m \frac{\partial q_m}{\partial t} + EI \sum_{m=1}^{\infty} \frac{\partial^4 W_m}{\partial z^4} q_m = \delta(z-L)F(t) \tag{A.3}$$

To remove the summation of all the modes, the equation of motion is multiplied with one mode shape[1], W_n, and integrated over the full length, see equation A.4. The different modes are orthogonal, meaning that this operation results in a value of zero if $m \neq n$. Therefore, only one mode remains, the mode where $m = n$.
By removing the brackets and putting the different terms into seperate integrals, equation A.5 is obtained. Since $q_n(t)$ is independent of z, it can be removed from the integral, giving equation A.6. This equation directly gives the formulas for the modal quantities, which are shown in equation A.7.

$$\begin{gathered} \int_0^L W_n(EoM)\,dz \\ \int_0^L W_n(\rho A W_n \frac{\partial^2 q_n}{\partial t^2} + cW_n\frac{\partial q_n}{\partial t} + EI\frac{\partial^4 W_n}{\partial z^4} q_n = \delta(z-L)F(t))\,dz \end{gathered} \tag{A.4}$$

$$\int_0^L W_n \rho A W_n \frac{\partial^2 q_n}{\partial t^2}\,dz + \int_0^L W_n c W_n \frac{\partial q_n}{\partial t}\,dz + \int_0^L W_n EI \frac{\partial^4 W_n}{\partial z^4} q_n\,dz = \int_0^L W_n \delta(z-L)F(t))\,dz \tag{A.5}$$

[1] This is the mode for which the modal quantities have to be determined.

$$\int_0^L W_n \rho A W_n \, dz \, \frac{\partial^2 q_n}{\partial t^2} + \int_0^L W_n c W_n \, dz \frac{\partial q_n}{\partial t} + \int_0^L W_n EI \frac{\partial^4 W_n}{\partial z^4} \, dz \, q_n = \int_0^L W_n \delta(z-L) F(t) \, dz$$

$$\int_0^L W_n \rho A W_n \, dz \, \frac{\partial^2 q_n}{\partial t^2} + \int_0^L W_n c W_n \, dz \frac{\partial q_n}{\partial t} + \int_0^L W_n EI \frac{\partial^4 W_n}{\partial z^4} \, dz \, q_n = W_n(L) F(t) \tag{A.6}$$

$$M_m \frac{\partial^2 q_n}{\partial t^2} + C_m \frac{\partial q_n}{\partial t} + K_m q_n = F_m(t)$$

$$\begin{aligned} M_m &= \int_0^L W_n \rho A W_n \, dz \\ C_m &= \int_0^L W_n c W_n \, dz \\ K_m &= \int_0^L W_n EI \frac{\partial^4 W_n}{\partial z^4} \, dz \\ F_m(t) &= W_n(L) F(t) \end{aligned} \tag{A.7}$$

A.2. Modal damping from damping ratio

The damping ratio is defined as the damping divided by the critical damping, see equation A.8. The critical damping for a mass spring system can be seen in equation A.9. The resulting modal damping can be seen in equation A.10

$$\zeta = C_m / C_r \tag{A.8}$$

$$C_r = 2\sqrt{M_m K_m} \tag{A.9}$$

$$C_m = 2\zeta\sqrt{M_m K_m} \tag{A.10}$$

B

Parameter A

This appendix gives an overview of the values of parameter A, used to describe the relation between the current in and the force produced by the actuator. Figure B.1 shows a graph of the value plotted against the frequency. Table B.1 gives the values with the corresponding frequencies.

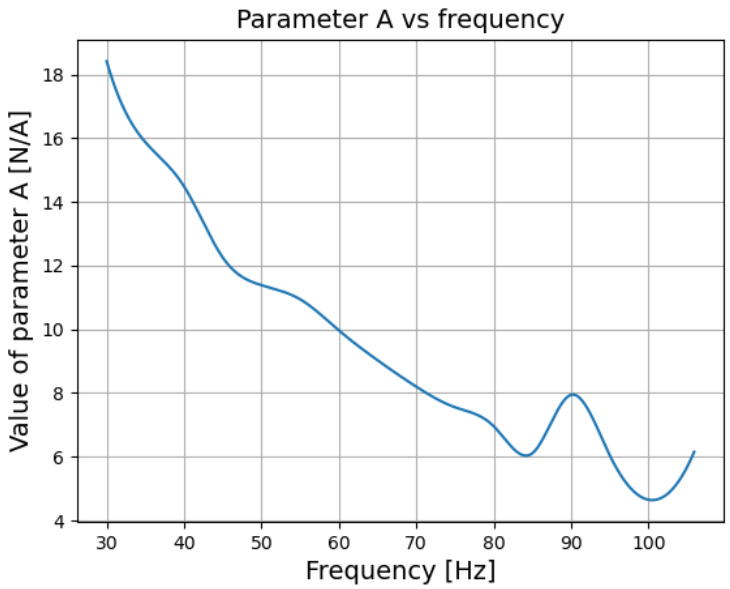

Figure B.1: Parameter A vs frequency

Frequency [Hz]	Parameter A [N/A]
30	18.415
35	15.875
40	14.488
45	12.254
50	11.387
55	10.943
60	9.968
65	9.030
70	8.200
75	7.555
80	6.960
85	6.114
90	7.946
95	6.043
100	4.654
105	5.689

Table B.1: Parameter A for different frequencies

C

Time series

This appendix shows the time series of different signals, for further comparison of the results.

C.1. Beam tip displacement

This section gives time series of the frequency sweeps that were performed, for both the open-loop and the closed-loop tests.

C.1.1. Open-loop

Figures C.1 through C.6 show the time series of a frequency sweep performed at an input amplitude of 3 amperes, for the frequencies of 45 Hz, 47 Hz and 49 Hz.

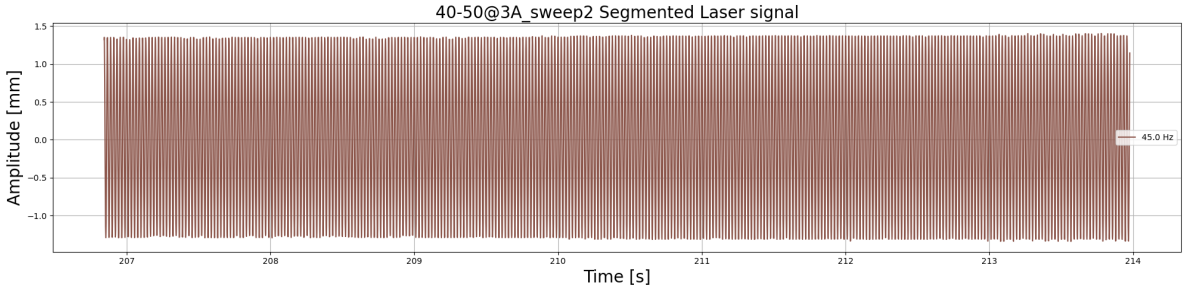

Figure C.1: Time series: open-loop at 3A at 45 Hz

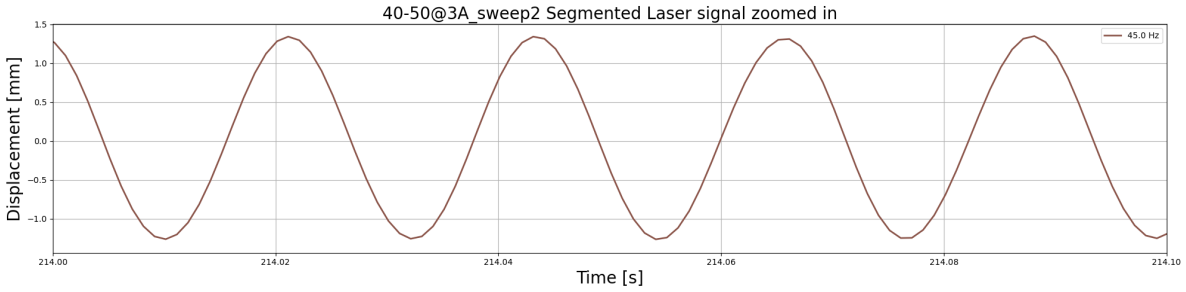

Figure C.2: Zoomed in time series: open-loop at 3A at 45 Hz

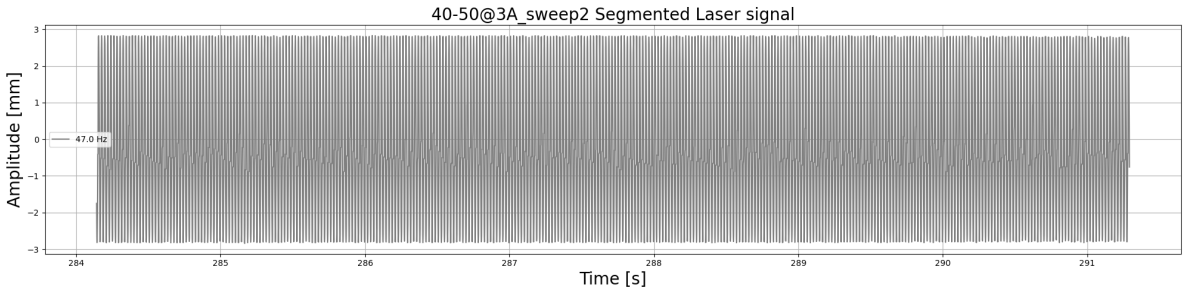

Figure C.3: Time series: open-loop at 3A at 47 Hz

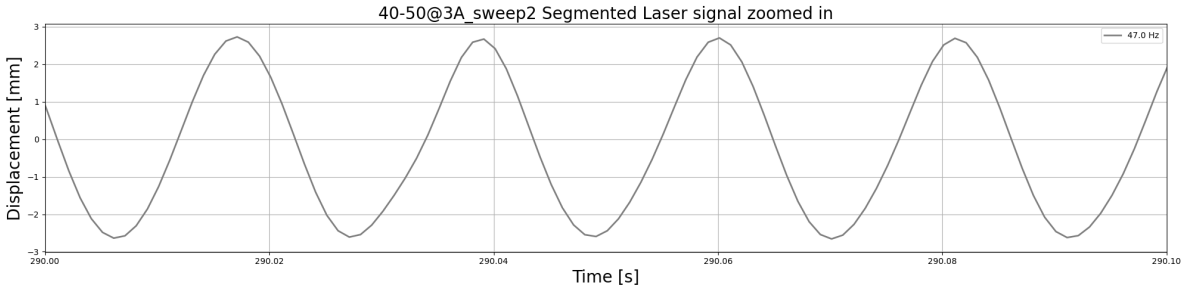

Figure C.4: Zoomed in time series: open-loop at 3A at 47 Hz

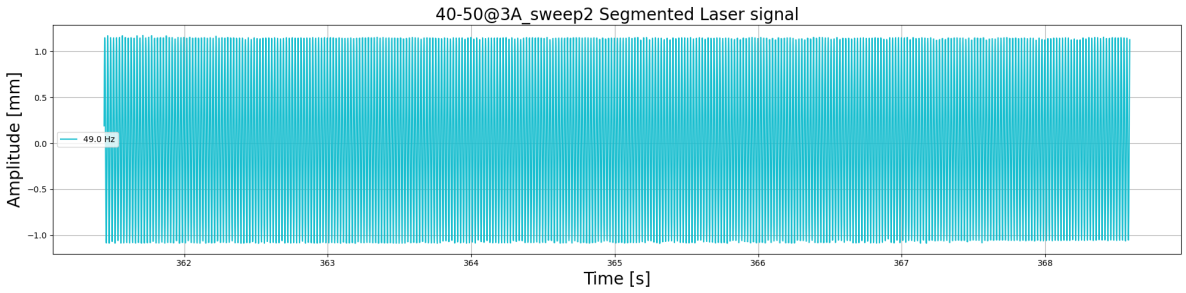

Figure C.5: Time series: open-loop at 3A at 49 Hz

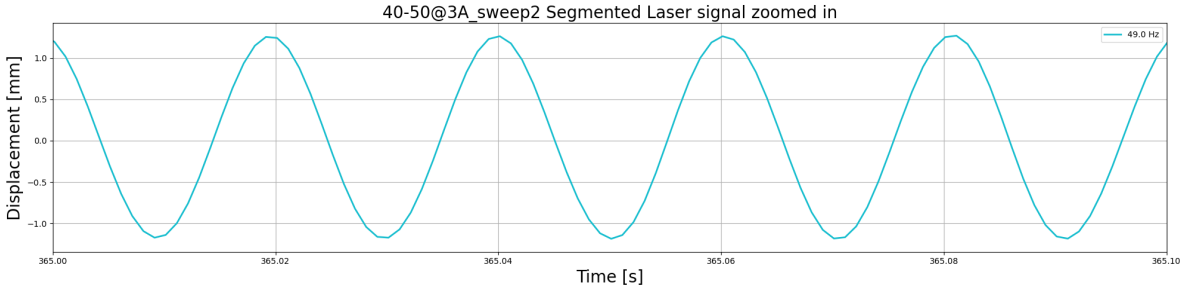

Figure C.6: Zoomed in time series: open-loop at 3A at 49 Hz

C.1.2. Closed-loop

Figures C.7 through C.12 show the time series of a frequency sweep performed at an input amplitude of 1 mm, for the frequencies of 41.5 Hz, 43.5 Hz and 45.5 Hz.

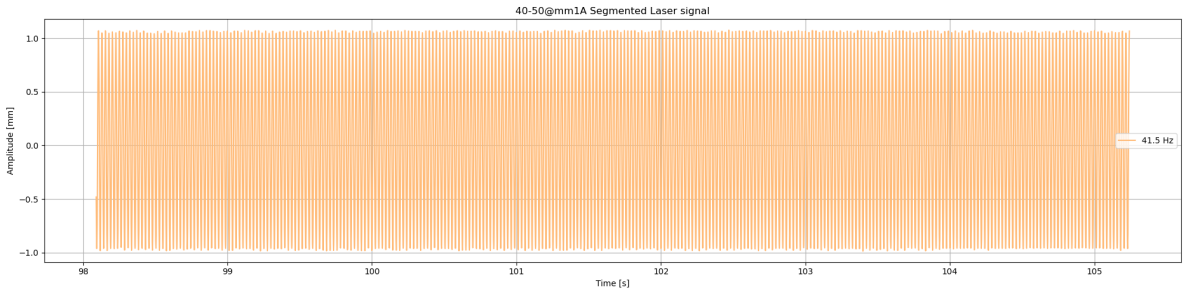

Figure C.7: Time series: closed-loop at 1 mm at 41.5 Hz

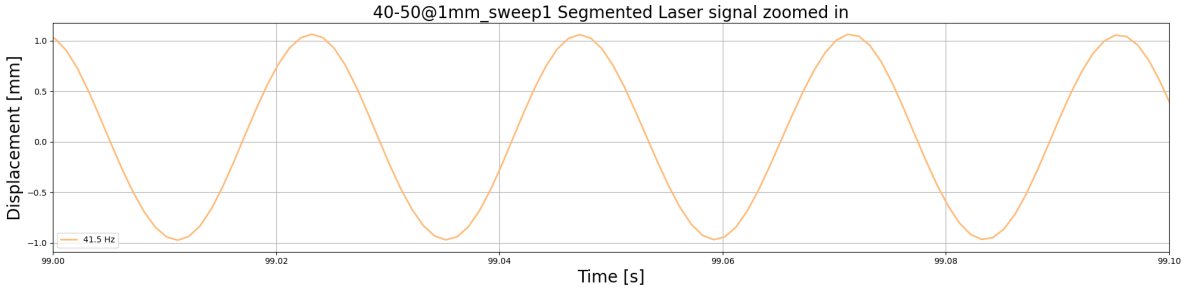

Figure C.8: Zoomed in time series: closed-loop at 1 mm at 41.5 Hz

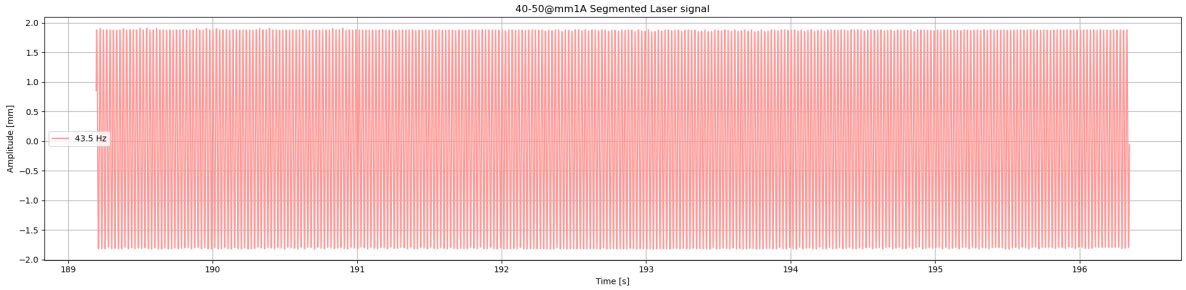

Figure C.9: Time series: closed-loop at 1 mm at 43.5 Hz

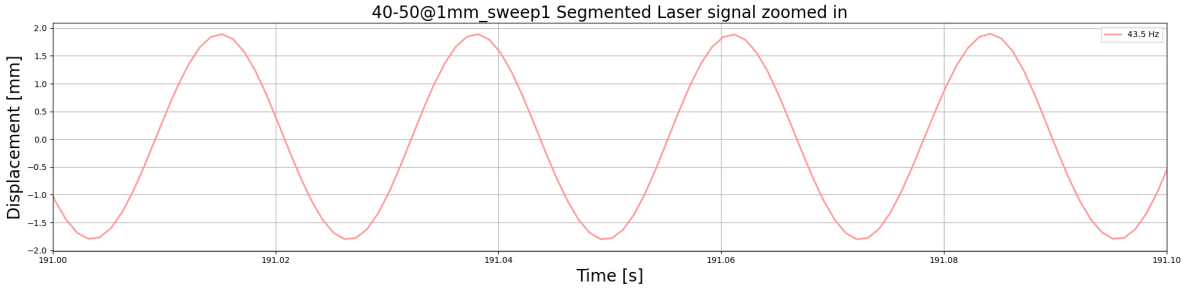

Figure C.10: Zoomed in time series: closed-loop at 1 mm at 43.5 Hz

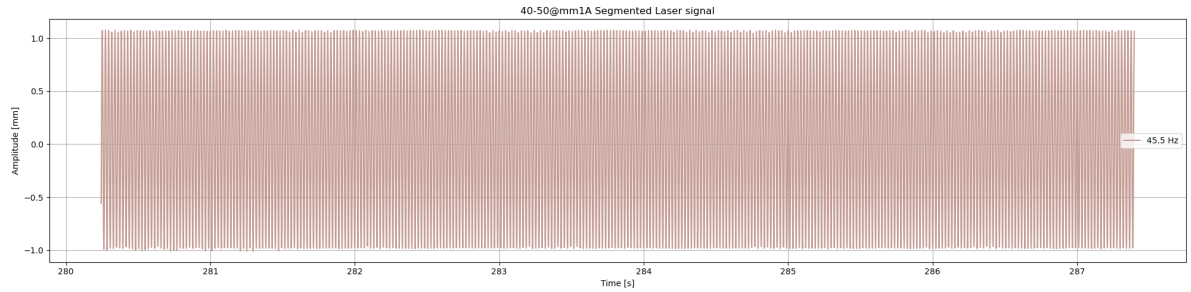

Figure C.11: Time series: closed-loop at 1 mm at 45.5 Hz

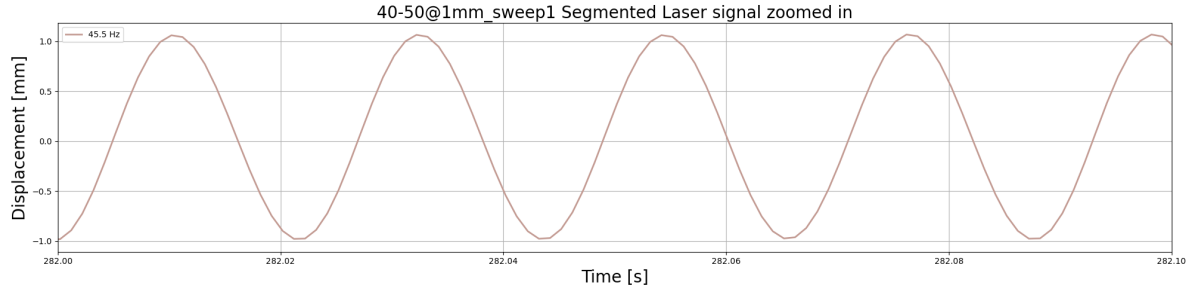

Figure C.12: Zoomed in time series: closed-loop at 1 mm at 45.5 Hz

C.2. Current in actuator

Figures C.13 and C.14 show time series of the current needed to create a smooth relative motion of the cylinder for the closed-loop setting at an input amplitude of 1 mm, for the experiments and the computer model respectively.

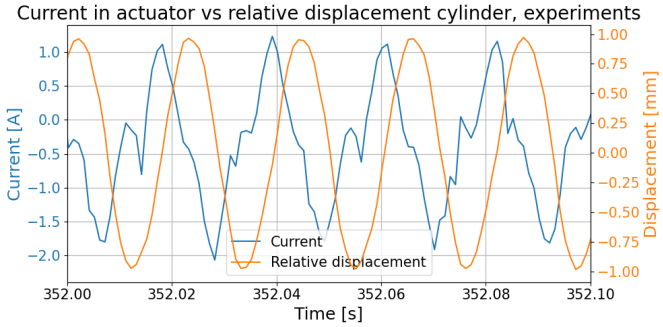

Figure C.13: Current vs relative displacement: experiments

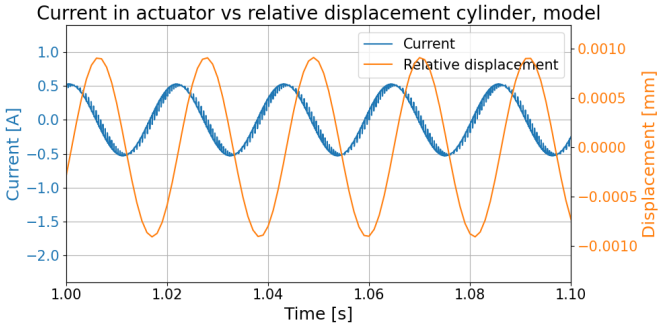

Figure C.14: Current vs relative displacement: model

D

First model results

This Appendix shows the results of the first version of the computer model. This version had a beam length of 1 m, instead of the later used 1.2 m. The beam tip displacement of both the model and the physical experiments can be seen in figure D.1. The graphs from the model show resonance peaks at 64 Hz, in contrast to the experiments, that have peaks at 47 Hz. In addition to the different frequency, the peaks from the model are also smaller than those from the experiments.

This difference could be the result of the model not accounting for the volume of the actuator. This means that in reality the centre of gravity of the actuator is higher than in the model. This gives the actuator force a larger arm. A larger torque is then created, resulting in larger displacements of the beam.

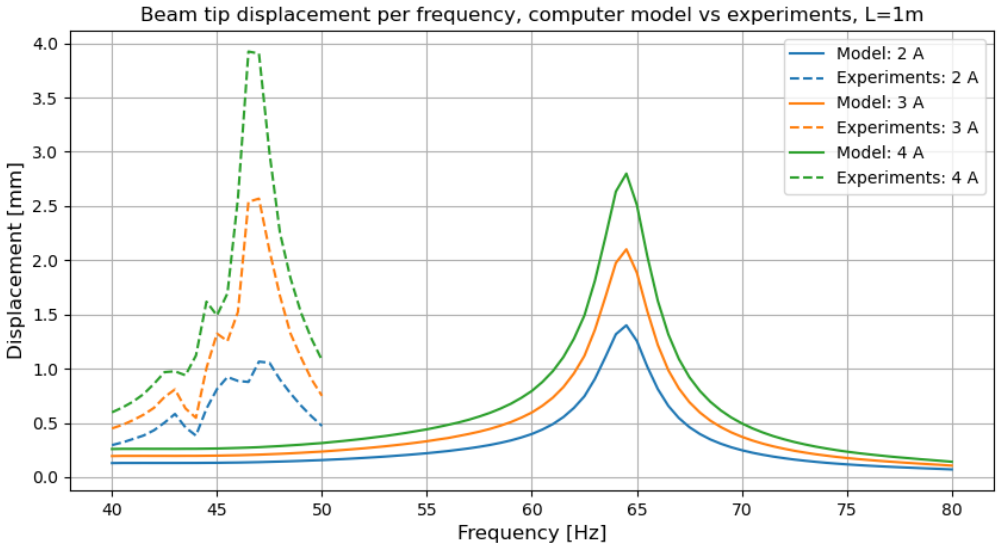

Figure D.1: First version model vs experiments for open-loop: Beam tip displacement